Physica D 239 (2010) 1083–1094

Contents lists available at ScienceDirect

Physica D

journal homepage: www.elsevier.com/locate/physd

On a special type of border-collision bifurcations occurring at infinity

Viktor Avrutin [a], Michael Schanz [a,*], Laura Gardini [b]

[a] Institute of Parallel and Distributed Systems, University of Stuttgart, Germany

[b] Department of Economics and Quantitative Methods, University of Urbino, Italy

ARTICLE INFO

Article history:
Received 24 September 2009
Received in revised form
16 February 2010
Accepted 27 February 2010
Available online 8 March 2010
Communicated by G. Stepan

Keywords:
Border-collision bifurcations
Piecewise-smooth maps
Piecewise-linear maps

ABSTRACT

In piecewise-smooth dynamical systems, the regions of existence of a periodic orbit are typically parameter sub-spaces confined by border-collision bifurcations of this orbit. We demonstrate that additionally to the usual border-collision bifurcations occurring at finite points in the state space there exist also border-collision bifurcations occurring at infinity.

1. Introduction

Piecewise-smooth dynamical systems are characterized by the fact that their state space is divided into partitions by borders also denoted as switching manifolds. Within each partition, the system is smooth (that is C^k up to some k) but the rules which govern the dynamic behavior (that is the right hand side of the system function) change at the boundaries. These systems are interesting because it was shown that they represent adequate mathematical models for many processes both in nature and engineering. Applications of these systems range from earthquake dynamics [1,2] to nano-actuators [3–6] and include electronic devices with relay or switching components (for example, buck/boost converters [7,8]), mechanical systems with stick–slip or impact phenomena [9,10] and in general all switching systems occurring in various fields as control theory [11], economics [12,13], biology [14] and so on. It is also worth noticing that the phenomenon of deterministic chaos represents a genuine source of such a switching behavior caused by the complicated stretching and folding mechanisms sometimes denoted as razor-blade or butterfly effect. This was demonstrated for example in [15] where the famous time-continuous smooth Lorenz flow [16] was investigated by means of a piecewise-smooth scalar map.

It is natural to ask which bifurcations occur in piecewise-smooth dynamical systems. Additionally, to all bifurcations occurring in smooth systems there is another class of bifurcations caused by the collision of an invariant set with a switching manifold. These bifurcations named by Nusse and Yorke [17] as border-collision bifurcations lead an invariant set (for example a fixed point or a periodic orbit) to be destroyed. However, it is also well known that there is another way for an invariant set to be destroyed, namely when some points of the set tend to infinity by variation of a parameter. Hence, the question arises how these bifurcations can be explained and whether they have some common properties with the "usual" border-collision bifurcations.

The key point of our paper goes back to the ideas suggested already by Poincaré [18] who has demonstrated that in order to obtain the global phase portrait of a flow it is necessary to investigate its behavior at infinity. Nowadays, the approach to include the dynamic behavior at infinity is called Poincaré compactification. When dealing with piecewise-smooth systems and especially with the bifurcations mentioned above, we will show that it is suitable to consider infinity a special kind of boundary in the state space. In doing so, the bifurcations occurring when some points of an invariant set tend to infinity turn out to be a kind of border-collision bifurcation. This has several advantages: on one hand, we can apply the knowledge already available for "usual" border-collision bifurcations and on the other hand it leads us to a unified description of bifurcations in piecewise-smooth systems.

This paper is organized as follows. In Section 2, we introduce the concept of Poincaré Equator (P.E.)-collision bifurcations and show why in piecewise-smooth systems these bifurcations can be seen as some kind of border-collision bifurcations. In Section 3, we prove that in the case of piecewise-linear maps an orbit undergoing a P.E.-collision bifurcation changes its stability. Eventually, in

* Corresponding author. Tel.: +49 7117816350.
E-mail addresses: Viktor.Avrutin@ipvs.uni-stuttgart.de (V. Avrutin), Michael.Schanz@ipvs.uni-stuttgart.de (M. Schanz), Laura.Gardini@uniurb.it (L. Gardini).

0167-2789/$ – see front matter © 2010 Elsevier B.V. All rights reserved.
doi:10.1016/j.physd.2010.02.015

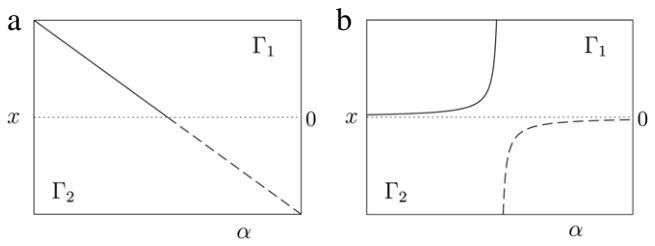

Fig. 1. Schematic representation of a border-collision bifurcation (a) and a P.E.-collision bifurcation (b) in a system defined on two partitions Γ_1 and Γ_2. Real orbits are shown as solid curves and virtual orbits as dashed curves.

Section 4, the results obtained so far will be applied to the well-known 2D piecewise-linear normal form. We demonstrate that the existence region of periodic orbits are bounded by the border-collision bifurcation curves which are (up to few exceptions) of the non-smooth fold type and by the P.E.-collision bifurcation curves which are of the transcritical type. Further, we present an explanation of the behavior at the codimension-2 bifurcation points where these curves intersect. Finally, in Section 5, we conclude with a summary.

2. Basic idea: how an orbit may become virtual?

For simplicity, let us consider a piecewise-smooth map $\mathcal{T}$ defined on two partitions in $\mathbb{R}^N$. Without a significant loss of generality, let us assume that the partitions are defined by the sign of the first state variable (that means $x < 0$ and $x > 0$)

$$\vec{X}_{n+1} = \mathcal{T}(\vec{X}_n, \alpha) = \begin{cases} \mathcal{T}_{\mathcal{L}}(\vec{X}_n, \alpha) & \text{if } x_n < 0 \\ \mathcal{T}_{\mathcal{R}}(\vec{X}_n, \alpha) & \text{if } x_n > 0 \end{cases} \tag{1}$$

with the state vector $\vec{X} = (x, y, \ldots)^T \in \mathbb{R}^N$ and a parameter $\alpha \in \mathbb{R}$. Let us further assume that the map has a fixed point $\vec{X}^*(\alpha) = (x^*(\alpha), y^*(\alpha), \ldots)^T$ given by a solution of the equation $\mathcal{T}_{\mathcal{R}}(\vec{X}, \alpha) = \vec{X}$. Obviously, $\vec{X}^*(\alpha)$ is a fixed point of the map (1) only if it is located in the partition where the function $\mathcal{T}_{\mathcal{R}}$ is valid, that means if $x^*(\alpha) > 0$. Otherwise, it represents a so-called virtual (non-existing) fixed point. Hence, the question how a real fixed point may become a virtual fixed point (or, in other words, may be destroyed) under variation of α reduces to the question how the scalar function $x^*(\alpha)$ may change its sign. The simplest possibility for that is a continuous transition across the boundary between partitions, given in our example by $x^*(\alpha) = 0$. This situation represents a usual border-collision bifurcation, shown schematically in Fig. 1(a). Several types of such bifurcations are well investigated so far (we refer to [8,19] for overviews).

However, there is still one more possibility for the function $x^*(\alpha) = 0$ to change its sign, namely the function may have a discontinuity, like for example a pole. In this case (see Fig. 1(b)), the fixed point tends to $+\infty$ as α approaches the critical value. After the parameter crossing of the critical value, the fixed point "returns" from $-\infty$. However, since the sign of $x^*(\alpha)$ is changed, in this case $\vec{X}^*(\alpha)$ represents a virtual fixed point, that means, it will be destroyed. Note that such kind of "infinity-crossing" may occur in systems defined on one partition as well, but in this case it does not cause the solution to be destroyed.[1]

[1] As an example, the reader may consider the behavior of the unstable fixed point $x = 1 - 1/\alpha$ of the logistic map $x_{n+1} = \alpha x_n(1 - x_n)$ at the parameter value $\alpha = 0$. An infinite sequence of such bifurcations where not only a fixed point but also the n-periodic orbits with any n undergo such bifurcation can be observed in the map $x_{n+1} = \alpha/(\alpha - x_n^2)$.

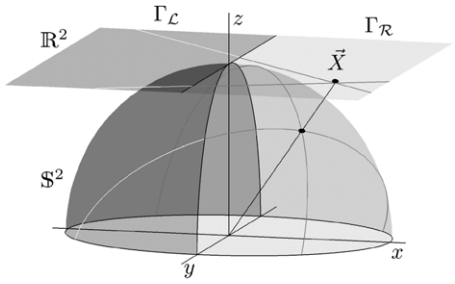

Fig. 2. Projection of a point $\vec{X}$ from the plane $\mathbb{R}^2$ onto the northern hemisphere of the Poincaré sphere $\mathbb{S}^2$.

Obviously, not only may a fixed point become virtual by such kind of bifurcation but any attractor and especially any periodic orbit. Furthermore, it is not significant that the map (1) is defined on two partitions only, since the described mechanism is valid for maps defined on an arbitrary number $M > 1$ of partitions in the state space. What is significant here, is the fact that the function representing the involved orbit in dependence on the parameter (for example, $x^*(\alpha)$) has a pole with an odd order, whereby the existence condition of the orbit is fulfilled on one side of the discontinuity and violated on the other side.

When dealing with orbits tending to infinity, the concept of the Poincaré compactification introduced in 1881 by Poincaré itself [18] is very useful. For an outline of this concept, we refer for example to [20,21]. Following Poincaré, this concept was applied by many authors to investigate the principal structure of phase portraits of certain dynamical systems including the branches tending to infinity (see for example [22–26]). According to this concept, the state space $\Gamma = \mathbb{R}^N$ is mapped by a central projection onto the northern hemisphere of the unit sphere $\mathbb{S}^N \subset \mathbb{R}^N$. Note that we use here the topological geometrical (and not the geometrical) convention of the sphere. Hereby, the origin of the space Γ corresponds to the north pole of the sphere $\mathbb{S}^N$ and the points at infinity in the space Γ are mapped onto the equator of the sphere, denoted as P.E.. This projection is illustrated in Fig. 2 for the case $N = 2$. The figure shows a point $\vec{X}$ located in the plane $\mathbb{R}^2$ and its projection onto the northern hemisphere of the Poincaré sphere $\mathbb{S}^2$. As one can easily see, for increasing $\|\vec{X}\|$ the projection of $\vec{X}$ is tending to the P.E. and each straight line in the plane is mapped onto a great circle of the sphere. Consequently, the boundary between the partitions $x < 0$ and $x > 0$ in $\mathbb{R}^2$ is mapped onto the great circle separating the two corresponding partitions on the sphere.

Let us reconsider the definition of the map (1). As the partitions (the domains of the partial maps $\mathcal{T}_{\mathcal{L}}$ and $\mathcal{T}_{\mathcal{R}}$) are specified by $x < 0$ and $x > 0$, one could assume that there exists only one boundary $x = 0$ between these partitions. However, the "infinity-crossings" discussed above lead us to the conclusion that $\pm\infty$ may represent partition boundaries as well. From a formal point of view, the partitions should be specified as

$$\Gamma_{\mathcal{L}} = \left\{\vec{X} \mid x \in (-\infty, 0)\right\} \quad \text{and} \quad \Gamma_{\mathcal{R}} = \left\{\vec{X} \mid x \in (0, +\infty)\right\} \tag{2}$$

whereby one partition boundary is given by the $(N-1)$-dimensional sub-space

$$\left\{\vec{X} \mid x = 0, \|\vec{X}\| < \infty\right\} \tag{3}$$

located at a finite value of x, and the other one, given by

$$\left\{\vec{X} \mid x = \pm\infty\right\} \tag{4}$$

is located at the P.E..

The key point of our work is given by the fact that the bifurcations occurring at both kinds of boundaries are similar. The situation where a bounded orbit collides with a finite partition boundary is in the meanwhile well known and represents a border-collision bifurcation. We state additionally that the same bifurcation occurs in the case when an orbit becomes unbounded and collides with a partition boundary at the P.E.. Formally, both bifurcations are border-collision bifurcations. However, for the sake of clarity, we want in the following to distinguish between them. Therefore, in the following, we keep the notation of a border-collision bifurcation for a collision with a finite boundary and denote a collision with an infinite boundary as a *P.E.-collision*. As in the case of a border-collision bifurcation, after a P.E.-collision bifurcation, the orbit becomes virtual. Similarly, several specific sub-types of border-collision bifurcations may occur at the P.E. as they may occur at finite partition boundaries.

3. Piecewise-linear case

In the discussion presented above, the partial maps $\mathcal{T}_{\mathcal{L}}$ and $\mathcal{T}_{\mathcal{R}}$ are not restricted to be of any specific type. However, it turns out that some additional results can be obtained for an important special case, namely for piecewise-linear maps. This class of models is known to be relevant for practical applications and is investigated by many authors (see references in [19]). Again, for the sake of clarity let us assume that the map is defined on two partitions in the state space as in the case of map (1):

$$\vec{X}_{n+1} = \begin{cases} A_{\mathcal{L}}\vec{X}_n + \vec{B}_{\mathcal{L}} & \text{if } x_n < 0 \\ A_{\mathcal{R}}\vec{X}_n + \vec{B}_{\mathcal{R}} & \text{if } x_n > 0 \end{cases} \tag{5}$$

where $A_{\mathcal{L}}$ and $A_{\mathcal{R}}$ are $N \times N$ matrices and $\vec{B}_{\mathcal{L}}, \vec{B}_{\mathcal{R}} \in \mathbb{R}^N$. Note that all the results presented below are valid also for maps defined on an arbitrary number $M > 1$ of partitions.

Throughout this paper, we use the following notation. For the orbits, we use one of the standard symbolic codings (see, for example, [27]) and denote a point $(x, y, \ldots)^T \in \mathbb{R}^N$ with $x < 0$ by the symbol $\mathcal{L}$ and a point with $x > 0$ by the symbol $\mathcal{R}$. A periodic orbit is denoted as O_σ, whereby the sequence $\sigma = \sigma_0\sigma_1 \ldots \sigma_{n-1}$ represents a cycle of period n (as described below). The regions in the parameter space where the orbit O_σ exists are denoted by $\mathcal{P}_\sigma^i$, where $i = 1, 2, \ldots$ is a index needed to distinguish between several regions. Each of these regions may consist of the parts $\mathcal{P}_\sigma^{i,s}$ and $\mathcal{P}_\sigma^{i,u}$ where the orbit O_σ is stable and unstable, respectively.

Let us consider a periodic orbit O_σ of system (5). The symbolic sequence σ of a cycle of period n is given by $\sigma_0\sigma_1\sigma_2 \ldots \sigma_{n-1}$, where each specific letter σ_i is $\mathcal{L}$ or $\mathcal{R}$ depending on the partition of the state space in which the corresponding point $\vec{X}_i^\sigma$ is located. Consequently, for each of these points Eq. (5) implies $\vec{X}_{i+1}^\sigma = A_{\sigma_i}\vec{X}_i^\sigma + \vec{B}_{\sigma_i}$ and especially

$$\vec{X}_1^\sigma = A_{\sigma_0}\vec{X}_0^\sigma + \vec{B}_{\sigma_0} \tag{6}$$

$$\vec{X}_2^\sigma = A_{\sigma_1}A_{\sigma_0}\vec{X}_0^\sigma + A_{\sigma_1}\vec{B}_{\sigma_0} + \vec{B}_{\sigma_1} \tag{7}$$

$$\vec{X}_3^\sigma = A_{\sigma_2}A_{\sigma_1}A_{\sigma_0}\vec{X}_0^\sigma + A_{\sigma_2}A_{\sigma_1}\vec{B}_{\sigma_0} + A_{\sigma_2}\vec{B}_{\sigma_1} + \vec{B}_{\sigma_2} \tag{8}$$

$$\ldots$$

$$\vec{X}_n^\sigma = \mathcal{A}^\sigma\vec{X}_0^\sigma + \vec{\mathcal{B}}^\sigma \quad \text{with } \mathcal{A}^\sigma = \prod_{i=1}^{n} A_{\sigma_{n-i}} \tag{9}$$

$$\vec{\mathcal{B}}^\sigma = \sum_{j=1}^{n-1}\left(\prod_{i=1}^{n-j} A_{\sigma_{n-i}}\right)\vec{B}_{\sigma_{j-1}} + \vec{B}_{\sigma_{n-1}}. \tag{10}$$

The periodicity condition $\vec{X}_n^\sigma = \vec{X}_0^\sigma$ for an orbit with period $n = |\sigma|$ leads finally to the following equation

$$(\mathcal{A}^\sigma - \mathcal{1})\vec{X}_0^\sigma = -\vec{\mathcal{B}}^\sigma \tag{11}$$

whereby $\mathcal{1}$ represents the $N \times N$ identity matrix. Recall that the solution of Eq. (11) – if it exists – leads to a true orbit of system (5), if all the points $\vec{X}_i^\sigma$ $(i = 0, \ldots, n-1)$ are located according to the symbolic sequence σ and to a virtual orbit otherwise. According to the Fredholm alternative, the following holds: either the matrix $(\mathcal{A}^\sigma - \mathcal{1})$ is invertible and hence Eq. (11) has a unique solution

$$\vec{X}_0^\sigma = -(\mathcal{A}^\sigma - \mathcal{1})^{-1}\vec{\mathcal{B}}^\sigma \tag{12}$$

representing the starting point of the orbit O_σ, or the matrix $(\mathcal{A}^\sigma - \mathcal{1})$ is not invertible and hence $\det(\mathcal{A}^\sigma - \mathcal{1}) = 0$, which means that $\lambda = 1$ is an eigenvalue of the matrix $\mathcal{A}^\sigma$. According to Cramer's rule the unique solution (12) of Eq. (11) satisfies the following equation

$$\det(\mathcal{A}^\sigma - \mathcal{1})\vec{X}_0^\sigma = -\vec{V} \tag{13}$$

whereby the i-th component of the vector $\vec{V}$ is given by $V_i = \det((\mathcal{A}^\sigma - \mathcal{1})_i)$ and the matrices $(\mathcal{A}^\sigma - \mathcal{1})_i$ are formed by replacing the i-th column of $(\mathcal{A}^\sigma - \mathcal{1})$ with the vector $\vec{\mathcal{B}}^\sigma$. Consequently, the denominator of each component of the solution vector $\vec{X}_0^\sigma$ is given by $\det(\mathcal{A}^\sigma - \mathcal{1})$. This means that the condition of a vanishing denominator implies that at least one eigenvalue of the matrix $\mathcal{A}^\sigma$ is $\lambda = 1$. Recall that due to the linearity of the system functions, the matrix $\mathcal{A}^\sigma$ represents the Jacobian matrix of the n-th iterated function at the point $\vec{X}_0^\sigma$ and hence is responsible for the stability of the n-periodic orbit O_σ considered above. Therefore, we conclude as a final result that *in the case of piecewise-linear maps like (5) the orbit O_σ undergoes a P.E.-collision bifurcation at the stability boundary, whereby exactly one eigenvalue of the matrix $\mathcal{A}^\sigma$ becomes* $+1$. Note that a hint towards this result was already mentioned in [28]. However, in the cited work, it was stated for a particular continuous piecewise-linear map. By contrast, the discussion presented above demonstrates that this result is valid also in general, both for continuous and discontinuous maps. Note further that we do not consider here the case of multiple eigenvalues.

Remarkably, the results obtained above for the general case of piecewise-linear maps in $\mathbb{R}^n$ can be easily illustrated for 1D maps. In Fig. 3(a) and (c), the situations before and after the bifurcation, respectively, are shown schematically for the case discussed in Section 2 with the additional condition that the partial system function $f_{\mathcal{R}}$ is linear. As one can see in Fig. 3(a), before the bifurcation the fixed point x^* defined by the solution of the equation $f_{\mathcal{R}}(x) = x$ is valid. As the system parameter approaches the bifurcation point, the fixed point tends to $+\infty$ and the slope tends to $+1$. At the bifurcation point (Fig. 3(b)), the slope is $+1$ and the equation $f_{\mathcal{R}}(x) = x$ has no finite solutions. After the bifurcation the solution exists again, but represents a virtual fixed point (Fig. 3(c)).

Let us now summarize the notation related to parameter subspaces (especially, curves in 2D parameter spaces) corresponding to specific bifurcations, which we will discuss in the following. The parameter sub-space, where an orbit O_σ undergoes a P.E. collision bifurcation will be denoted by χ_σ. The parameter sub-space where this orbit undergoes a border-collision bifurcation is denoted by $\xi_\sigma^{d,i}$, whereby the index $i \in [0, |\sigma|-1]$ refers to the fact that the i-th point of the orbit collides with the boundary in the state space. The superscript $d \in \{\mathcal{L}, \mathcal{R}\}$ represents the direction of the collision, that is whether the i-th point of the orbit O_σ collides with the border $x = 0$ from the left ($\mathcal{L}$) or from the right ($\mathcal{R}$). The stability boundaries of an orbit O_σ are denoted by θ_σ^+ and θ_σ^-, whereby the superscripts depend on the fact whether the stability boundary is caused by an eigenvalue equal to $+1$ or to -1, respectively.

4. Application example: 2D normal form

4.1. Definitions

To illustrate the ideas discussed above, let us consider the well-known 2D normal form

$$\vec{X}_{n+1} = \mathcal{T}(\vec{X}_n) = \begin{cases} \mathcal{T}_{\mathcal{L}}(\vec{X}_n) = A_{\mathcal{L}}\vec{X}_n + \vec{B} & \text{if } x_n < 0 \\ \mathcal{T}_{\mathcal{R}}(\vec{X}_n) = A_{\mathcal{R}}\vec{X}_n + \vec{B} & \text{if } x_n > 0 \end{cases} \tag{14}$$

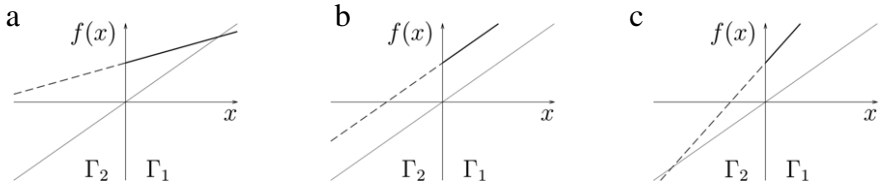

Fig. 3. Schematic representation of the P.E.-collision bifurcation of the fixed point x^*: Situations before the bifurcation (a), at the bifurcation point (b) and after the bifurcation (c). The partial system function $f_{\mathcal{R}}$ is shown as solid line within its domain and as dashed line outside.

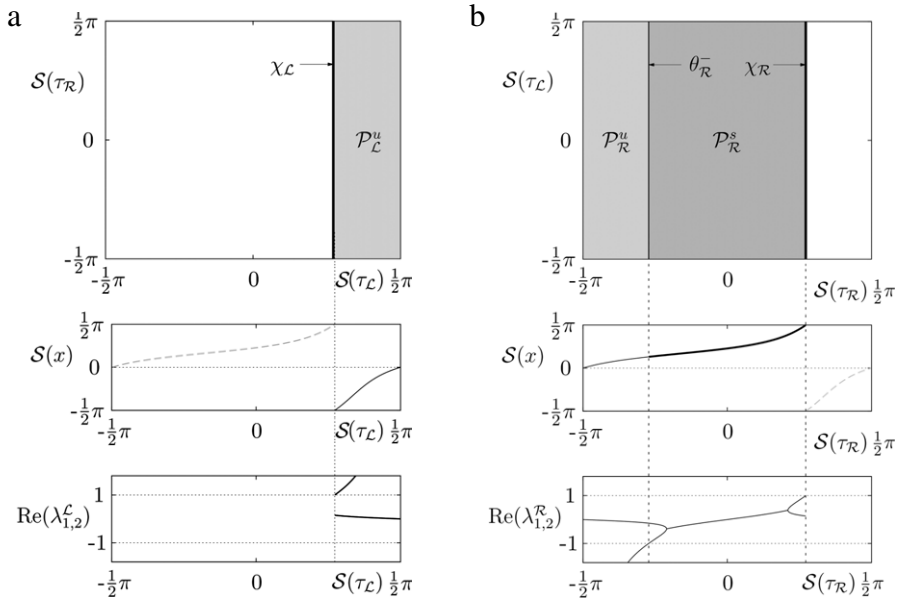

Fig. 4. Fixed points $O_{\mathcal{L}}$ (a) and $O_{\mathcal{R}}$ (b). In the bifurcation diagrams (middle row), thick lines show stable fixed points, thin lines – unstable fixed points and dashed lines – virtual fixed points. In the lower row, the corresponding eigenvalues are shown. Parameters: $\delta_{\mathcal{L}} = \delta_{\mathcal{R}} = 0.15$. Note that in (b) the parameter plane $(\tau_{\mathcal{R}}, \tau_{\mathcal{L}})$ and not $(\tau_{\mathcal{L}}, \tau_{\mathcal{R}})$ is shown which is in contrast to all other figures throughout this paper.

$$\text{with } A_{\mathcal{L}} = \begin{pmatrix} \tau_{\mathcal{L}} & 1 \\ -\delta_{\mathcal{L}} & 0 \end{pmatrix} \qquad A_{\mathcal{R}} = \begin{pmatrix} \tau_{\mathcal{R}} & 1 \\ -\delta_{\mathcal{R}} & 0 \end{pmatrix}$$

$$\vec{B} = \begin{pmatrix} \mu \\ 0 \end{pmatrix} \qquad \vec{X} = \begin{pmatrix} x \\ y \end{pmatrix}$$

proposed in the pioneering work by Nusse and Yorke [17], where the term "border-collision bifurcation" was introduced. Later, this map was investigated by many authors in a large number of works (see for example [29–33,8] and also the References in [19]). In the recent publications [34,35], it is shown that in the vicinity of specific bifurcation curves in the 2D parameter space of several nonlinear systems the bifurcation structure can be mapped onto the bifurcation structure of the normal form (14) using the normal form reduction described in [36,37,33]. Note additionally, that for $\delta_{\mathcal{L}} = \delta_{\mathcal{R}} = 0$ the map will be reduced to the 1D normal form:

$$x_{n+1} = \begin{cases} \tau_{\mathcal{L}} x_n + \mu & \text{if } x_n < 0 \\ \tau_{\mathcal{R}} x_n + \mu & \text{if } x_n > 0 \end{cases} \tag{15}$$

as mentioned already in [38]. It was shown in the cited work that under variation of the parameter μ, this map demonstrates transitions from a fixed point to several periodic orbits and to one- and multi-band chaotic attractors. Remarkably, for $\mu \neq 0$ by rescaling the variables via the transformation $\tilde{x} = x/|\mu|, \tilde{y} = y/|\mu|$ the dimension of the parameter space of map (14) can be reduced by one, and it is sufficient to consider only the three parameter values $\mu \in \{+1, 0, -1\}$. Additionally, it can easily be shown that the cases $\mu = +1$ and $\mu = -1$ are identical up to an exchange of $\tau_{\mathcal{L}}$ with $\tau_{\mathcal{R}}$ and $\delta_{\mathcal{L}}$ with $\delta_{\mathcal{R}}$ and of the signs of the variables. Consequently, in the following, we consider the case $\mu = 1$ only, and drop the tilde in the notation for the variables.

4.2. Fixed points and period-2 orbits

Let us firstly recall some results concerning the map (14) already mentioned for example in [38]. The map has two fixed points $O_{\mathcal{L}}$ and $O_{\mathcal{R}}$ given by

$$O_{\mathcal{L}/\mathcal{R}} = \left(\frac{\mu}{D^{\mathcal{L}/\mathcal{R}}}, \frac{-\delta_{\mathcal{L}/\mathcal{R}}\mu}{D^{\mathcal{L}/\mathcal{R}}} \right)^T$$

$$\text{with } D^{\mathcal{L}/\mathcal{R}} = 1 - \tau_{\mathcal{L}/\mathcal{R}} + \delta_{\mathcal{L}/\mathcal{R}} \tag{16}$$

where the notation "$\mathcal{L}/\mathcal{R}$" means "$\mathcal{L}$ or $\mathcal{R}$". Each of the fixed points exists iff it is located in the corresponding partition, that means iff $O_{\mathcal{L}} \in \Gamma_{\mathcal{L}}$ and $O_{\mathcal{R}} \in \Gamma_{\mathcal{R}}$. The stability of both fixed points is determined by the eigenvalues

$$\lambda_{1,2}^{\mathcal{L}/\mathcal{R}} = \frac{1}{2}\left(\tau_{\mathcal{L}/\mathcal{R}} \pm \sqrt{\tau_{\mathcal{L}/\mathcal{R}}^2 - 4\delta_{\mathcal{L}/\mathcal{R}}} \right) \tag{17}$$

of the matrices $A_{\mathcal{L}}$ and $A_{\mathcal{R}}$. The regions of existence and stability of the fixed points $O_{\mathcal{L}/\mathcal{R}}$ are shown in Fig. 4, whereby for a better graphical representation in this and all further figures we use the mapping

$$\mathcal{S}(\nu) : (-\infty, \infty) \mapsto (-\pi/2, \pi/2), \quad \text{with } \mathcal{S}(\nu) = \arctan(\nu) \tag{18}$$

which allows us to present the structure of the state and parameter space in the complete range from $-\infty$ to ∞. Since the tangent function increases strictly monotonic, the scaling $\mathcal{S}$ preserves the topological structure of the displayed space.

As one can see in Fig. 4, the fixed points $O_{\mathcal{L}/\mathcal{R}}$ do not undergo border-collision bifurcations. This is obvious, since we assumed $\mu \neq 0$ and hence the numerator of the x-component in Eq. (16) cannot become zero. Instead, for any $\delta_{\mathcal{L}/\mathcal{R}}$ the existence regions of

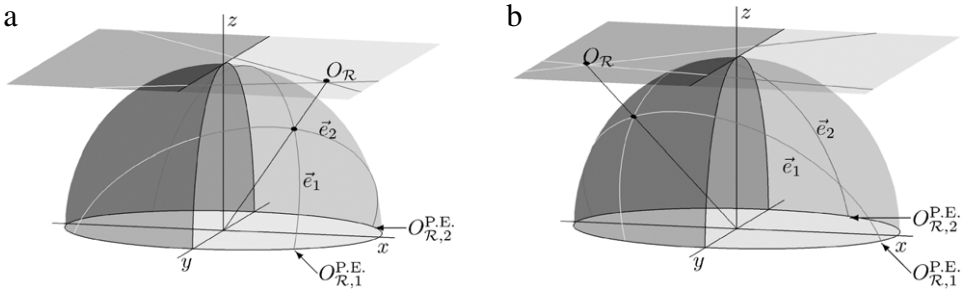

Fig. 5. Schematic representation of the fixed points $O^{\mathrm{P.E.}}_{\mathcal{R},1}$ and $O^{\mathrm{P.E.}}_{\mathcal{R},2}$ which are located at the P.E. and induced by the eigenvectors $\vec{e}_{1,2}$ of the finite fixed point $O_{\mathcal{R}}$. The fixed point is real in (a) and virtual in (b). The eigenvectors are shown as dark gray curves where they are real and as light gray curves where they are virtual.

the fixed points $O_{\mathcal{L}/\mathcal{R}}$ are bounded by the curves in the $(\tau_{\mathcal{L}}, \tau_{\mathcal{R}})$ parameter plane

$$\chi_{\mathcal{L}/\mathcal{R}} = \left\{(\tau_{\mathcal{L}}, \tau_{\mathcal{R}}) \mid D^{\mathcal{L}/\mathcal{R}} = 0\right\} \tag{19}$$

where the fixed points become virtual via a P.E.-collision bifurcation. Recall, that the values $\vartheta(x) = \pm\pi/2$ shown in Fig. 4 correspond to $x = \pm\infty$. As one can see, both fixed points, the stable $(O_{\mathcal{R}})$ and the unstable $(O_{\mathcal{L}})$ one undergo the P.E.-collision bifurcation, whereby at the bifurcation point one of the eigenvalues approaches the values $+1$, as expected according to the results of Section 3.

It can be shown that the P.E.-collision leading the fixed points to be destroyed represents a transcritical border-collision bifurcation occurring at the P.E.. Note that using the equation $\vec{X} = \mathcal{T}(\vec{X})$ directly, it is possible to calculate only the finite fixed points $O_{\mathcal{R}}$ and $O_{\mathcal{L}}$, whereas the map (14) has four further fixed points located at the P.E., two of them caused by $O_{\mathcal{R}}$ and the other two by $O_{\mathcal{L}}$ as follows from the explanations presented in the Appendix. The technique for their calculation, the so-called Poincaré compactification, is briefly discussed in Appendix. As shown there, fixed points on the P.E. of a linear map are the limit points of the eigenvectors issuing from finite fixed points. In Fig. 5(a), this is illustrated schematically for the fixed point $O_{\mathcal{R}}$. The eigenvectors $\vec{e}_{1,2}$ issuing from $O_{\mathcal{R}}$ connect this finite fixed point with the fixed points $O^{\mathrm{P.E}}_{\mathcal{R},1}$ and $O^{\mathrm{P.E}}_{\mathcal{R},2}$ located on the P.E.. As follows from Eq. (16), the fixed point $O_{\mathcal{R}}$ always belongs to the line $y = -\delta_{\mathcal{R}} x$ and the slopes of the eigenvectors $\vec{e}_{1,2}$ issuing from $O_{\mathcal{R}}$ are (see the Appendix) $m_{1,2} = -\delta_{\mathcal{R}}/\lambda^{\mathcal{R}}_{1,2}$, where the eigenvalues $\lambda^{\mathcal{R}}_{1,2}$ are given by Eq. (17). As long as $|\lambda^{\mathcal{R}}_{1,2}| < 1$ holds, both eigenvectors $\vec{e}_{1,2}$ represent stable eigenvectors for $O_{\mathcal{R}}$ and consequently unstable eigenvectors for $O^{\mathrm{P.E}}_{\mathcal{R},1}$ and $O^{\mathrm{P.E}}_{\mathcal{R},2}$. However, if the parameters are varied across the curve $\chi_{\mathcal{R}}$, then the eigenvalue $\lambda^{\mathcal{R}}_1$ reaches the value $+1$, the fixed point $O_{\mathcal{R}}$ is merging with the fixed point $O^{\mathrm{P.E}}_{\mathcal{R},1}$ on the P.E. and a "change of stability" takes place: $O_{\mathcal{R}}$ becomes unstable, whereas $O^{\mathrm{P.E}}_{\mathcal{R},1}$ becomes stable. Additionally, since the map is piecewise linear, after the bifurcation the fixed point $O_{\mathcal{R}}$ becomes not only unstable but *virtual*. Anyhow, the two eigenvectors issuing from this virtual fixed point exist in the region $\Gamma_{\mathcal{R}}$ and the related limit points are fixed points on the P.E., as shown in Fig. 5(b). In particular, the fixed point $O^{\mathrm{P.E}}_{\mathcal{R},1}$ representing the limit point of the unstable eigenvector $\vec{e}_1$ of the unstable virtual fixed point $O_{\mathcal{R}}$ after the bifurcation is an attractor on the P.E..

So far, we have shown that the bifurcation occurring at the curve

$$\theta^{+}_{\mathcal{R}} = \{(\tau_{\mathcal{L}}, \tau_{\mathcal{R}}) \mid \lambda^{\mathcal{R}}_1 = +1\} \equiv \chi_{\mathcal{R}} \tag{20}$$

is a transcritical bifurcation on the P.E. (the fixed points $O_{\mathcal{R}}$ and $O^{\mathrm{P.E}}_{\mathcal{R},1}$ merge and interchange the stability) with an additional feature that one of the involved fixed points becomes virtual after the bifurcation. In order to explain what happens at the other stability boundary

$$\theta^{-}_{\mathcal{R}} = \left\{(\tau_{\mathcal{L}}, \tau_{\mathcal{R}}) \mid \lambda^{\mathcal{R}}_2 = -1\right\} \tag{21}$$

we have to consider not only the fixed point $O_{\mathcal{R}}$ but also the period-2 orbit $O_{\mathcal{R}\mathcal{L}}$. Using Eq. (12), we get for the points of the $O_{\mathcal{R}\mathcal{L}}$ orbit:

$$x^{\mathcal{R}\mathcal{L}}_i = \frac{N^{\mathcal{R}\mathcal{L}}_i}{D^{\mathcal{R}\mathcal{L}}}, \qquad y^{\mathcal{R}\mathcal{L}}_i = \frac{M^{\mathcal{R}\mathcal{L}}_i}{D^{\mathcal{R}\mathcal{L}}}, \quad i = 0, 1 \tag{22a}$$

with

$$N^{\mathcal{R}\mathcal{L}}_0 = \mu(1 + \delta_{\mathcal{L}} + \tau_{\mathcal{L}}), \qquad M^{\mathcal{R}\mathcal{L}}_0 = -\delta_{\mathcal{L}} N^{\mathcal{R}\mathcal{L}}_1 \tag{22b}$$

$$N^{\mathcal{R}\mathcal{L}}_1 = \mu(1 + \delta_{\mathcal{R}} + \tau_{\mathcal{R}}), \qquad M^{\mathcal{R}\mathcal{L}}_1 = -\delta_{\mathcal{R}} N^{\mathcal{R}\mathcal{L}}_0 \tag{22c}$$

$$D^{\mathcal{R}\mathcal{L}} = 1 + \delta_{\mathcal{L}} + \delta_{\mathcal{R}} + \delta_{\mathcal{L}}\delta_{\mathcal{R}} - \tau_{\mathcal{L}}\tau_{\mathcal{R}}. \tag{22d}$$

Note that the points given by Eqs. (22a) represent a real orbit $O_{\mathcal{R}\mathcal{L}}$ only if the corresponding condition of existence is fulfilled, which is given by

$$x^{\mathcal{R}\mathcal{L}}_0 > 0, \qquad x^{\mathcal{R}\mathcal{L}}_1 < 0. \tag{23}$$

Otherwise, these points represent a virtual orbit. The stability of the orbit $O_{\mathcal{R}\mathcal{L}}$ is determined by the eigenvalues

$$\lambda^{\mathcal{R}\mathcal{L}}_{1,2} = \frac{1}{2}\Big(\tau_{\mathcal{L}}\tau_{\mathcal{R}} - \delta_{\mathcal{L}} - \delta_{\mathcal{R}} \pm \sqrt{(\tau_{\mathcal{L}}\tau_{\mathcal{R}} - (\delta_{\mathcal{L}} + \delta_{\mathcal{R}}))^2 - 4\delta_{\mathcal{L}}\delta_{\mathcal{R}}}\Big) \tag{24}$$

of the Jacobian matrix $\mathcal{A}^{\mathcal{R}\mathcal{L}} = A_{\mathcal{L}}A_{\mathcal{R}}$. The regions of existence and stability of the orbit $O_{\mathcal{R}\mathcal{L}}$ are shown in Fig. 6. Note that the region of existence of the orbit $O_{\mathcal{R}\mathcal{L}}$ consists of two parts. The first region $\mathcal{P}^1_{\mathcal{R}\mathcal{L}}$ itself includes the two sub-regions $\mathcal{P}^{1,s}_{\mathcal{R}\mathcal{L}}$ and $\mathcal{P}^{1,u}_{\mathcal{R}\mathcal{L}}$, separated by the stability boundary

$$\theta^{-}_{\mathcal{R}\mathcal{L}} = \left\{(\tau_{\mathcal{L}}, \tau_{\mathcal{R}}) \mid \lambda^{\mathcal{R}\mathcal{L}}_2 = -1\right\}. \tag{25}$$

In the second region $\mathcal{P}^2_{\mathcal{R}\mathcal{L}} \equiv \mathcal{P}^{2,u}_{\mathcal{R}\mathcal{L}}$ the orbit $O_{\mathcal{R}\mathcal{L}}$ is unstable and coexists with the stable fixed point $O^{s}_{\mathcal{R}}$. As one can see, the outer boundaries of the regions $\mathcal{P}^1_{\mathcal{R}\mathcal{L}}$ and $\mathcal{P}^2_{\mathcal{R}\mathcal{L}}$ are given by bifurcation curves of both types, namely by the usual border-collision curve

$$\xi^{\mathcal{L},1}_{\mathcal{R}\mathcal{L}} = \left\{(\tau_{\mathcal{L}}, \tau_{\mathcal{R}}) \mid N^{\mathcal{R}\mathcal{L}}_1 = 0\right\} \tag{26}$$

where the point $x^{\mathcal{R}\mathcal{L}}_1$ collides with the finite boundary $x = 0$ and by the P.E.-collision bifurcation curve

$$\chi_{\mathcal{R}\mathcal{L}} = \left\{(\tau_{\mathcal{L}}, \tau_{\mathcal{R}}) \mid D^{\mathcal{R}\mathcal{L}} = 0\right\}. \tag{27}$$

Our next task is to determine the types of bifurcations occurring at the curves $\xi^{\mathcal{L},1}_{\mathcal{R}\mathcal{L}}$ and $\chi_{\mathcal{R}\mathcal{L}}$. From Eqs. (17), (22c) and (26) we obtain that the condition $N^{\mathcal{R}\mathcal{L}}_1 = 0$ implies $\lambda^{\mathcal{R}}_2 = -1$.

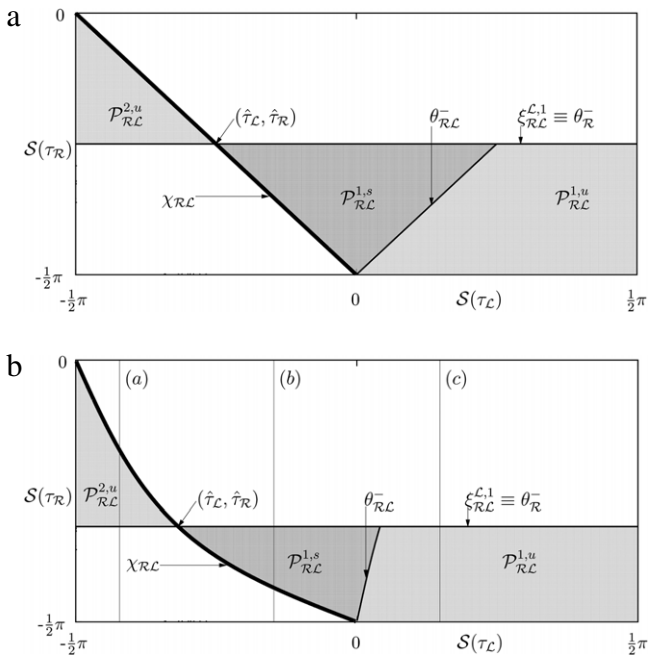

Fig. 6. Period-2 orbits $O_{\mathcal{RL}}$ for $\delta_{\mathcal{L}} = \delta_{\mathcal{R}} = 0$ (a) and $\delta_{\mathcal{L}} = \delta_{\mathcal{R}} = 0.55$ (b). The vertical segments marked in (b) with letters (a), (b) and (c) correspond to the three bifurcation diagrams shown in Fig. 7.

Consequently, the curves $\xi^{\mathcal{L},1}_{\mathcal{RL}}$ and $\theta^{-}_{\mathcal{R}}$ coincide and represent a degenerate flip bifurcation,[2] as shown in Fig. 7. Remarkably, the first two cases shown in Fig. 7(a) and (b) resemble sub- and supercritical flip bifurcations, whereas the third case (Fig. 7(c)) is different and corresponds in this case to the transition from a stable fixed point to a chaotic attractor. Note additionally that exactly at the bifurcation point, we observe a continuum of coexisting neutral period-2 orbits located on the eigenvector of the fixed point $O_{\mathcal{R}}$ corresponding to the eigenvalue $\lambda = -1$ (see [40]). These orbits form the vertical segments at the bifurcation points shown in Fig. 7.

To understand the situation with the P.E.-collision curve $\chi_{\mathcal{RL}}$ note that for the two-cycle we can reason as for a fixed point. In fact, the two points of the orbit $O_{\mathcal{RL}}$ are fixed for the second iterated of the map $\mathcal{T}$, that is the point of the two-cycle located in $\Gamma_{\mathcal{R}}$ (respectively, in $\Gamma_{\mathcal{L}}$) is a fixed point of the map $\mathcal{T}_{\mathcal{L}} \circ \mathcal{T}_{\mathcal{R}}$ (respectively, of the map $\mathcal{T}_{\mathcal{R}} \circ \mathcal{T}_{\mathcal{L}}$). The eigenvectors issuing from these fixed points have limit values, which give two-cycles on the P.E.. It is easy to see that for example the point of the two-cycle located in the region $\Gamma_{\mathcal{L}}$ belongs to the line of slope $s = -(\delta_{\mathcal{R}}\tau_{\mathcal{L}})/(1 + \delta_{\mathcal{R}})$, which is also the slope of the eigenvector associated with the eigenvalue $\lambda = 1$ on the bifurcation value. Thus, the two-cycle $O_{\mathcal{RL}}$ is merging with the two-cycle on the P.E. which is attracting after the bifurcation, when the real two-cycle $O_{\mathcal{RL}}$ changes the stability (that means, $\lambda_1^{\mathcal{RL}} = +1$ as follows from the results of Section 3) and becomes virtual. Consequently, the P.E.-collision bifurcation $\chi_{\mathcal{RL}}$ represents a transcritical bifurcation at the P.E..

It is worth noting that the whole region $\mathcal{P}^{2,u}_{\mathcal{RL}}$ is a region, where a variation of μ from a positive value to zero leads to dangerous border-collision bifurcations [41,28,42,43]. Recall that these bifurcation occur if there are some bounded attractors[3] which coexist with divergent trajectories (so that there is at least one attractor also on the P.E.) and for parameters tending to the bifurcation value the basins of attraction of these attractors shrink to zero. As a consequence of that, at the point of a dangerous bifurcation the behavior for all typical initial values is divergent, while the attractor at the P.E. is almost global. In the region $\mathcal{P}^{2,u}_{\mathcal{RL}}$, the basin of the attractor on the P.E. is separated from the basin of the stable fixed point $O^{s}_{\mathcal{R}}$ by the stable manifold of the unstable cycle $O^{u}_{\mathcal{RL}}$. Consequently, as μ tends to zero the area of the basin of $O^{s}_{\mathcal{R}}$ tends to zero as well. Note that regions of dangerous bifurcation are typically bounded by P.E.-collision bifurcation curves of unstable orbits. For example, in the region $1 - \delta_{\mathcal{R}} < \tau_{\mathcal{R}} < -1 - \delta_{\mathcal{R}}$, $\tau_{\mathcal{L}} > 1 - \delta_{\mathcal{L}}$ which is bounded from the left by the P.E.-collision bifurcation curve $\chi_{\mathcal{L}}$, the basin of the stable fixed point $O^{s}_{\mathcal{R}}$ is separated from the basin of the attractor on the P.E by the stable manifold of the unstable fixed point $O^{u}_{\mathcal{L}}$. Hence, varying μ to zero we observe a dangerous border-collision bifurcation also in this region.

Increasing $\delta_{\mathcal{L}/\mathcal{R}}$ from zero to a positive value, we observe that the situation with the fixed points and with the period-2 orbit $O_{\mathcal{RL}}$ does not change significantly. Comparing Fig. 6(a) and (b), we conclude that the shapes of the regions $\mathcal{P}^{1,2}_{\mathcal{RL}}$ change but the overall bifurcation structure remains the same. As we will see in the next section, for other periodic orbits this is not the case.

4.3. Pairs of complementary orbits $O_{\mathcal{RL}^n}$ and $O_{\mathcal{R}^2\mathcal{L}^{n-1}}$

As for many other dynamical systems, for system (14) the period-2 orbit $O_{\mathcal{RL}}$ considered in the previous section represents a special case. In order to demonstrate a more generic case, let us consider other periodic orbits of system (14). Let us first recall the situation for $\delta_{\mathcal{L}/\mathcal{R}} = 0$ which corresponds – as already mentioned – to the 1D map (15). Here, only one family of stable periodic orbits exists, namely the family $O_{\mathcal{RL}^n}$ with $n \geq 1$, typically denoted as maximal [44,45] or basic [46] orbits.[4] By contrast, for $\delta_{\mathcal{L}/\mathcal{R}} > 0$ system (14) shows further families of stable periodic orbits, for example $O_{\mathcal{R}^n\mathcal{L}^2}$ and $O_{\mathcal{R}^2\mathcal{L}(\mathcal{RL})^n}$. However, for the aims of this paper it is sufficient to consider the basic orbits, whereas an investigation of other families remains for future work. For the basic orbits, Eq. (12) can be written in the compact form

$$\vec{X}_0^{\mathcal{RL}^n} = -\left(A_{\mathcal{L}}^n A_{\mathcal{R}} - \mathcal{I}\right)^{-1} \left(\sum_{i=0}^{n} A_{\mathcal{L}}^i\right) \vec{B} \tag{28}$$

and the remaining n points $X_i^{\mathcal{RL}^n}$ with $i = 1, \ldots, n$ can be calculated by forward iteration of this point.

First, let us consider the most simple case of orbits from the $O_{\mathcal{RL}^n}$-family, namely the 3-periodic orbit $O_{\mathcal{RL}^2} = \{(x_i^{\mathcal{RL}^2}, y_i^{\mathcal{RL}^2})^T \mid i = 0, 1, 2\}$. Using Eq. (28), we obtain the points of this orbit:

$$x_i^{\mathcal{RL}^2} = \frac{N_i^{\mathcal{RL}^2}}{D^{\mathcal{RL}^2}}, \qquad y_i^{\mathcal{RL}^2} = \frac{M_i^{\mathcal{RL}^2}}{D^{\mathcal{RL}^2}}, \quad i = 0, 1, 2 \tag{29a}$$

with

$$N_0^{\mathcal{RL}^2} = \mu(1 - \delta_{\mathcal{L}} + \tau_{\mathcal{L}} + \delta_{\mathcal{L}}^2 + \tau_{\mathcal{L}}^2 + \tau_{\mathcal{L}}\delta_{\mathcal{L}}),$$
$$M_0^{\mathcal{RL}^2} = -\delta_{\mathcal{L}} N_2^{\mathcal{RL}^2} \tag{29b}$$

[2] As shown in [39] (Theorem 3.5.1), when an eigenvalue crosses the value -1 in a locally smooth map with negative (respectively, positive) Schwarzian derivative, then the bifurcation is called supercritical (respectively, subcritical), while in the case of zero Schwarzian derivative (as for linear and linear-fractional maps) the bifurcation is called degenerate. It is worth noticing that this case is associated with a continuum of coexisting cycles with doubled period at the bifurcation point [40].

[3] In the original publications [41,28], dangerous border-collision bifurcations are discussed for fixed points. However, there is no reason to restrict the consideration to fixed points only. Thus, we will speak about dangerous bifurcations of any bounded attractors in the same sense as it is done in [43].

[4] Recall that we consider here the case $\mu > 0$. Of course, the existence of the orbits $O_{\mathcal{RL}^n}$ for $\mu > 0$ implies the existence of the orbits $O_{\mathcal{LR}^n}$ for $\mu < 0$.

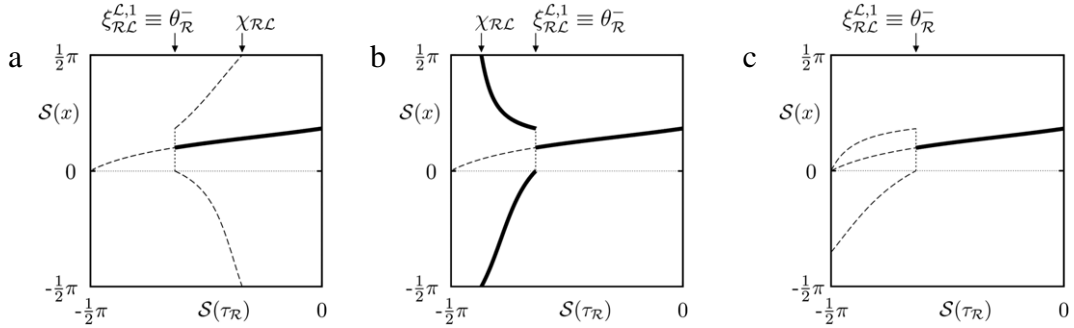

Fig. 7. Fixed point $O_{\mathcal{R}}$ and period-2 orbit $O_{\mathcal{RL}}$ involved into degenerate flip bifurcations. Stable orbits are shown as solid curves and unstable as dashed curves. Dotted vertical lines show a continuum of neutral period-2 orbits coexisting at the bifurcation point. Parameter values: $\delta_{\mathcal{L}} = \delta_{\mathcal{R}} = 0.55$. $\tau_{\mathcal{L}} = -4$ (a), $\tau_{\mathcal{L}} = -0.5$ (b), $\tau_{\mathcal{L}} = 0.5$ (c).

$$N_1^{\mathcal{RL}^2} = \mu(\tau_{\mathcal{L}}\tau_{\mathcal{R}} + \tau_{\mathcal{L}}\delta_{\mathcal{R}} + \tau_{\mathcal{R}} + \delta_{\mathcal{L}}\delta_{\mathcal{R}} - \delta_{\mathcal{L}} + 1),$$

$$M_1^{\mathcal{RL}^2} = -\delta_{\mathcal{R}} N_0^{\mathcal{RL}^2} \tag{29c}$$

$$N_2^{\mathcal{RL}^2} = \mu(\tau_{\mathcal{L}}\tau_{\mathcal{R}} + \tau_{\mathcal{L}} + \tau_{\mathcal{R}}\delta_{\mathcal{L}} + \delta_{\mathcal{L}}\delta_{\mathcal{R}} - \delta_{\mathcal{R}} + 1),$$

$$M_2^{\mathcal{RL}^2} = -\delta_{\mathcal{L}} N_1^{\mathcal{RL}^2} \tag{29d}$$

$$D^{\mathcal{RL}^2} = 1 + \delta_{\mathcal{L}}\tau_{\mathcal{L}} + \delta_{\mathcal{L}}\tau_{\mathcal{R}} + \delta_{\mathcal{R}}\tau_{\mathcal{L}} + \delta_{\mathcal{L}}^2\delta_{\mathcal{R}} - \tau_{\mathcal{L}}^2\tau_{\mathcal{R}}. \tag{29e}$$

As usual, the points given by Eq. (29a) represent a real orbit iff the corresponding condition of existence

$$x_0^{\mathcal{RL}^2} > 0, \qquad x_1^{\mathcal{RL}^2} < 0, \qquad x_2^{\mathcal{RL}^2} < 0 \tag{30}$$

is fulfilled and a virtual orbit otherwise. The stability of the orbit $O_{\mathcal{RL}^2}$ is determined by the eigenvalues of the Jacobian matrix $\mathcal{A}^{\mathcal{RL}^2} = A_{\mathcal{L}}^2 A_{\mathcal{R}}$, which are given by

$$\lambda_{1,2}^{\mathcal{RL}^2} = \frac{1}{2}\left(\tau_{\mathcal{L}}^2\tau_{\mathcal{R}} - \tau_{\mathcal{L}}\delta_{\mathcal{L}} - \tau_{\mathcal{L}}\delta_{\mathcal{R}} - \tau_{\mathcal{R}}\delta_{\mathcal{L}} \pm \sqrt{H^{\mathcal{RL}^2}}\right) \tag{31a}$$

$$\begin{aligned} H^{\mathcal{RL}^2} = {} & \tau_{\mathcal{L}}^4\tau_{\mathcal{R}}^2 - 2\tau_{\mathcal{L}}^3\tau_{\mathcal{R}}\delta_{\mathcal{L}} - 2\tau_{\mathcal{L}}^3\tau_{\mathcal{R}}\delta_{\mathcal{R}} - 2\tau_{\mathcal{L}}^2\tau_{\mathcal{R}}^2\delta_{\mathcal{L}} \\ & + 2\tau_{\mathcal{L}}^2\delta_{\mathcal{L}}\delta_{\mathcal{R}} + \tau_{\mathcal{L}}^2\delta_{\mathcal{L}}^2 + \tau_{\mathcal{L}}^2\delta_{\mathcal{R}}^2 + 2\tau_{\mathcal{L}}\tau_{\mathcal{R}}\delta_{\mathcal{L}}^2 \\ & + 2\tau_{\mathcal{L}}\tau_{\mathcal{R}}\delta_{\mathcal{L}}\delta_{\mathcal{R}} + \tau_{\mathcal{R}}^2\delta_{\mathcal{L}}^2 - 4\delta_{\mathcal{L}}^2\delta_{\mathcal{R}}. \end{aligned} \tag{31b}$$

So far, a complete description of the orbit $O_{\mathcal{RL}^2}$ is obtained. The resulting shape of the region $\mathcal{P}^1_{\mathcal{RL}^2}$ in the case $\delta_{\mathcal{L}} = \delta_{\mathcal{R}} = 0$ is shown in Fig. 8(a). The boundary of this region is given by the border-collision curve $\xi^{\mathcal{L},2}_{\mathcal{RL}^2}$, where the point $x_2^{\mathcal{RL}^2}$ collides with the boundary $x = 0$

$$\xi^{\mathcal{L},2}_{\mathcal{RL}^2} = \left\{(\tau_{\mathcal{L}}, \tau_{\mathcal{R}}) \mid N_2^{\mathcal{RL}^2} = 0\right\} \tag{32}$$

which follows from Eq. (29d) with the additional condition (30), which guarantees that the orbit $O_{\mathcal{RL}^2}$ is real. The region $\mathcal{P}^1_{\mathcal{RL}^2}$ consists of the parts $\mathcal{P}^{1,s}_{\mathcal{RL}^2}$ and $\mathcal{P}^{1,u}_{\mathcal{RL}^2}$ where the orbit is stable and unstable, respectively. These parts are separated by the stability boundary $\theta^-_{\mathcal{RL}^2}$ given by

$$\theta^-_{\mathcal{RL}^2} = \left\{(\tau_{\mathcal{L}}, \tau_{\mathcal{R}}) \mid \lambda_2^{\mathcal{RL}^2} = -1\right\}. \tag{33}$$

It is not difficult to demonstrate that the border-collision bifurcation $\xi^{\mathcal{L},2}_{\mathcal{RL}^2}$ represents a non-smooth fold bifurcation, also known as non-smooth saddle–node bifurcation[5] or annihilation of the orbits on the boundary [33]. To this end, it is sufficient to calculate the existence and stability regions of the periodic orbit

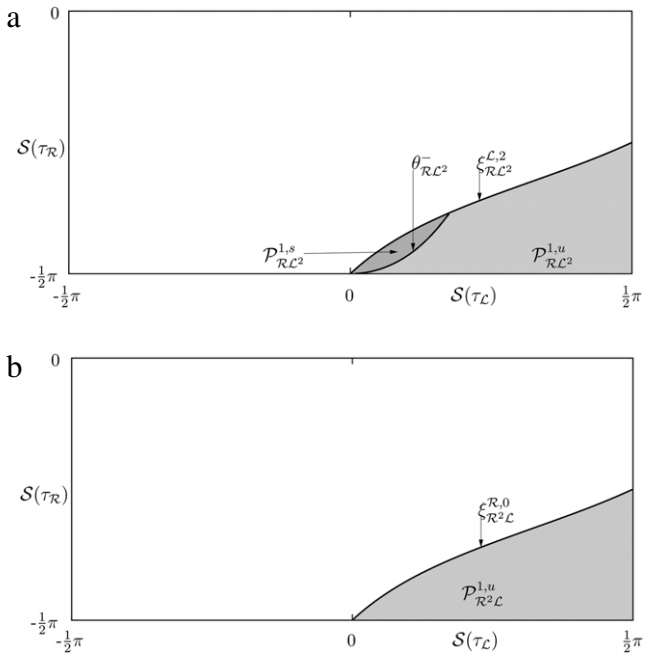

Fig. 8. Regions of existence of the period-3 orbits $O_{\mathcal{RL}^2}$ (a) and $O_{\mathcal{R}^2\mathcal{L}}$ (b) in the $(\tau_{\mathcal{L}}, \tau_{\mathcal{R}})$ parameter sub-space for $\delta_{\mathcal{L}} = \delta_{\mathcal{R}} = 0$.

complementary to $O_{\mathcal{RL}^2}$. For the concept of complementary orbits, we refer to [28]. According to this work, two orbits are called complementary to each other if their symbolic sequences differ by one letter, whereby this letter corresponds to those points of the orbits which collide with the boundary.

Especially for the family of basic orbits $O_{\mathcal{RL}^n}$, the family of complementary orbits is given[6] by $O_{\mathcal{R}^2\mathcal{L}^{n-1}}$. Hence, the orbit

[5] We remark that both the terms non-smooth fold and even more non-smooth saddle–node are quite misleading. In the theory of smooth bifurcations where this term originates from, a saddle–node bifurcation is known to occur at the parameter values where an eigenvalue of the involved orbits is $+1$ and the stability of the orbits emerging at the bifurcation point is different (in the 2D case we may have an attracting node and a saddle, or a saddle and a repelling node). By contrast, in the non-smooth case the bifurcation is not associated with an eigenvalue $+1$ and the stability of the emerging orbits is not necessarily different, so for example in the 2D case it may cause two saddle orbits to emerge [19]. Remarkable, this definition is not commonly accepted – in some publications the term non-smooth fold is restricted to the bifurcations where the stability of the involved orbits is as in the smooth case. However, we use the term non-smooth fold in the sense of [19].

[6] Note that the family of orbits complementary to the $O_{\mathcal{RL}^n}$ can be written also as $O_{\mathcal{RL}^{n-1}\mathcal{R}}$. In this case, for each specific n both orbits undergo a border-collision bifurcation whereby they collide with the boundary $x = 0$ with their last points. However, for convenience we will use in the following the more usual symbolic sequences $\mathcal{R}^2\mathcal{L}^{n-1}$, which are shift-invariant to $\mathcal{RL}^{n-1}\mathcal{R}$. Consequently, at the bifurcation the orbit $O_{\mathcal{RL}^n}$ collides with the boundary by its last point, whereas the orbit $O_{\mathcal{R}^2\mathcal{L}^{n-1}}$ collides with the boundary with its first point.

complementary to $O_{\mathcal{RL}^2}$ is $O_{\mathcal{R}^2\mathcal{L}}$. Straight forward calculations show that its points are given by

$$x_i^{\mathcal{R}^2\mathcal{L}} = \frac{N_i^{\mathcal{R}^2\mathcal{L}}}{D^{\mathcal{R}^2\mathcal{L}}}, \qquad y_i^{\mathcal{R}^2\mathcal{L}} = \frac{M_i^{\mathcal{R}^2\mathcal{L}}}{D^{\mathcal{R}^2\mathcal{L}}}, \quad i = 0, 1, 2 \tag{34a}$$

with

$$N_0^{\mathcal{R}^2\mathcal{L}} = \mu(\delta_{\mathcal{L}}\tau_{\mathcal{R}} + \tau_{\mathcal{L}} + 1 + \tau_{\mathcal{L}}\tau_{\mathcal{R}} + \delta_{\mathcal{R}}\delta_{\mathcal{L}} - \delta_{\mathcal{R}}),$$

$$M_0^{\mathcal{R}^2\mathcal{L}} = -\delta_{\mathcal{L}} N_2^{\mathcal{R}^2\mathcal{L}} \tag{34b}$$

$$N_1^{\mathcal{R}^2\mathcal{L}} = \mu(\tau_{\mathcal{L}}\tau_{\mathcal{R}} + \tau_{\mathcal{R}} + \delta_{\mathcal{R}}\delta_{\mathcal{L}} - \delta_{\mathcal{L}} + 1 + \tau_{\mathcal{L}}\delta_{\mathcal{R}}),$$

$$M_1^{\mathcal{R}^2\mathcal{L}} = -\delta_{\mathcal{R}} N_0^{\mathcal{R}^2\mathcal{L}} \tag{34c}$$

$$N_2^{\mathcal{R}^2\mathcal{L}} = \mu(\tau_{\mathcal{R}}^2 - \delta_{\mathcal{R}} + \delta_{\mathcal{R}}^2 + 1 + \delta_{\mathcal{R}}\tau_{\mathcal{R}} + \tau_{\mathcal{R}}),$$

$$M_2^{\mathcal{R}^2\mathcal{L}} = -\delta_{\mathcal{L}} N_1^{\mathcal{R}^2\mathcal{L}} \tag{34d}$$

$$D^{\mathcal{R}^2\mathcal{L}} = 1 + \delta_{\mathcal{R}}\tau_{\mathcal{R}} + \delta_{\mathcal{L}}\tau_{\mathcal{R}} - \tau_{\mathcal{L}}\tau_{\mathcal{R}}^2 + \tau_{\mathcal{L}}\delta_{\mathcal{R}} + \delta_{\mathcal{L}}\delta_{\mathcal{R}}^2 \tag{34e}$$

and its stability is determined by the eigenvalues

$$\lambda_{1,2}^{\mathcal{R}^2\mathcal{L}} = \frac{1}{2}\left(\tau_{\mathcal{L}}\tau_{\mathcal{R}}^2 - \delta_{\mathcal{R}}\tau_{\mathcal{R}} - \delta_{\mathcal{L}}\tau_{\mathcal{R}} - \tau_{\mathcal{L}}\delta_{\mathcal{R}} \pm \sqrt{H^{\mathcal{R}^2\mathcal{L}}}\right) \tag{35a}$$

$$\begin{aligned} H^{\mathcal{R}^2\mathcal{L}} = {} & \tau_{\mathcal{L}}^2\tau_{\mathcal{R}}^4 - 2\tau_{\mathcal{L}}\tau_{\mathcal{R}}^3\delta_{\mathcal{R}} - 2\tau_{\mathcal{L}}\tau_{\mathcal{R}}^3\delta_{\mathcal{L}} - 2\tau_{\mathcal{L}}^2\tau_{\mathcal{R}}^2\delta_{\mathcal{R}} \\ & + \delta_{\mathcal{R}}^2\tau_{\mathcal{R}}^2 + 2\delta_{\mathcal{R}}\tau_{\mathcal{R}}^2\delta_{\mathcal{L}} + 2\delta_{\mathcal{R}}^2\tau_{\mathcal{R}}\tau_{\mathcal{L}} + \delta_{\mathcal{L}}^2\tau_{\mathcal{R}}^2 \\ & + 2\tau_{\mathcal{L}}\delta_{\mathcal{R}}\delta_{\mathcal{L}}\tau_{\mathcal{R}} + \tau_{\mathcal{L}}^2\delta_{\mathcal{R}}^2 - 4\delta_{\mathcal{L}}\delta_{\mathcal{R}}^2 \end{aligned} \tag{35b}$$

of the matrix $A_{\mathcal{R}}^2 A_{\mathcal{L}}$. In the case $\delta_{\mathcal{L}/\mathcal{R}} = 0$, the orbit $O_{\mathcal{R}^2\mathcal{L}}$ is unstable in the complete region of existence $\mathcal{P}_{\mathcal{R}^2\mathcal{L}}$ and the only bifurcation involving this orbit is the border-collision bifurcation $\xi_{\mathcal{R}^2\mathcal{L}}^{\mathcal{R},0}$. Straight forward calculations show that this curve coincides with the border-collision bifurcation curve $\xi_{\mathcal{RL}^2}^{\mathcal{L},2}$, which represents consequently a non-smooth fold bifurcation as expected.

Note that in the case $\delta_{\mathcal{L}/\mathcal{R}} = 0$, the shapes of the regions of existence for each pair of complementary orbits $O_{\mathcal{RL}^n}$ and $O_{\mathcal{R}^2\mathcal{L}^{n-1}}$ with $n > 2$ are similar to the shapes of the regions $\mathcal{P}_{\mathcal{RL}^2}^1$ and $\mathcal{P}_{\mathcal{R}^2\mathcal{L}}^1$ shown in Fig. 8. Each pair of orbits $O_{\mathcal{RL}^n}$ and $O_{\mathcal{R}^2\mathcal{L}^{n-1}}$ emerges at the non-smooth fold bifurcation curve $\xi_{\mathcal{RL}^n}^{\mathcal{L},n} \equiv \xi_{\mathcal{R}^2\mathcal{L}^{n-1}}^{\mathcal{R},0}$, whereby the orbit $O_{\mathcal{RL}^n}$ may be either a stable node or a saddle, while the orbit $O_{\mathcal{R}^2\mathcal{L}^{n-1}}$ is unstable in its complete region of existence. Hence, the bifurcation curve $\xi_{\mathcal{RL}^n}^{\mathcal{L},n} \equiv \xi_{\mathcal{R}^2\mathcal{L}^{n-1}}^{\mathcal{R},0}$ represents in fact a non-smooth saddle–node bifurcation on the left side of its intersection point with the stability boundary $\theta_{\mathcal{RL}^n}^-$ and could be denoted as a non-smooth saddle–saddle bifurcation on the right side. However, we use in both cases the notation non-smooth fold bifurcation. Remarkably, this explains also the differences between the orbit $O_{\mathcal{RL}}$ and all other orbits from the $O_{\mathcal{RL}^n}$ family. Namely, the orbit $O_{\mathcal{RL}}$ does not have a complementary orbit and hence cannot be involved into a non-smooth fold bifurcation. Instead, $O_{\mathcal{RL}}$ emerges at a degenerate flip bifurcation as described above.

So far, we have shown that in the case $\delta_{\mathcal{L}/\mathcal{R}} = 0$ system (14) does not demonstrate P.E.-collision bifurcations involving basic orbits. It can be easily shown that the points of these orbits tend to the P.E. only for parameter values tending to the point $(\tau_{\mathcal{L}}, \tau_{\mathcal{R}}) = (0, -\infty)$. Since in the case $\delta_{\mathcal{L}/\mathcal{R}} = 0$, the only periodic orbits which may be stable are basic orbits, there are no P.E.-collision bifurcations involving stable periodic orbits for finite parameter values. By contrast, increasing $\delta_{\mathcal{L}/\mathcal{R}}$ from zero to a positive value we observe that this situation changes significantly. As one can see in Fig. 9(a), in this case each of the orbits $O_{\mathcal{RL}^2}$ and $O_{\mathcal{R}^2\mathcal{L}}$ exist in two regions. Similar to the case $\delta_{\mathcal{L}/\mathcal{R}} = 0$, the region $\mathcal{P}_{\mathcal{RL}^2}^1$ is separated into a stable and an unstable part by the curve $\theta_{\mathcal{RL}^2}^-$, whereas the orbit $O_{\mathcal{R}^2\mathcal{L}}$ is unstable in the complete region $\mathcal{P}_{\mathcal{R}^2\mathcal{L}}^1$. However, for $\delta_{\mathcal{L}/\mathcal{R}} > 0$ the boundaries of the region $\mathcal{P}_{\mathcal{RL}^2}^1$ are given by two bifurcation curves. Additionally, to the non-smooth fold bifurcation curve $\xi_{\mathcal{RL}^2}^{\mathcal{L},2} \equiv \xi_{\mathcal{R}^2\mathcal{L}}^{\mathcal{R},0}$ we observe the P.E.-collision bifurcation curve

$$\chi_{\mathcal{RL}^2} = \left\{(\tau_{\mathcal{L}}, \tau_{\mathcal{R}}) \mid D^{\mathcal{RL}^2} = 0\right\}. \tag{36}$$

Not only the stable orbit $O_{\mathcal{RL}^2}$ but also the unstable orbit $O_{\mathcal{R}^2\mathcal{L}}$ undergoes a P.E.-collision bifurcation occurring at the curve

$$\chi_{\mathcal{R}^2\mathcal{L}} = \left\{(\tau_{\mathcal{L}}, \tau_{\mathcal{R}}) \mid D^{\mathcal{R}^2\mathcal{L}} = 0\right\}. \tag{37}$$

Remarkably, the border-collision bifurcation curve $\xi_{\mathcal{RL}^2}^{\mathcal{L},2} \equiv \xi_{\mathcal{R}^2\mathcal{L}}^{\mathcal{R},0}$ intersects both P.E.-collision bifurcation curves $\chi_{\mathcal{RL}^2}$ and $\chi_{\mathcal{R}^2\mathcal{L}}$ at the same point, which is marked in Fig. 9 by $(\hat{\tau}_{\mathcal{L}}^1, \hat{\tau}_{\mathcal{R}}^1)$. The behavior at this codimension-2 bifurcation point is described in Section 4.4. It is worth noting that the equations of the bifurcation curves $\chi_{\mathcal{RL}}$ and $\chi_{\mathcal{R}^2\mathcal{L}}$ were already given in [28], although without any connection with the bifurcation on the P.E., while the equation of $\chi_{\mathcal{RL}^2}$ was already given in [42] noticing that it is associated with a transcritical bifurcation on the P.E..

As one can see in Fig. 9, there exists a region $\mathcal{P}_{\mathcal{R}^2\mathcal{L}}^1 \setminus \mathcal{P}_{\mathcal{RL}^2}^1$ between the P.E.-collision bifurcation curves, where the orbit $O_{\mathcal{RL}^2}$ is already destroyed but the orbit $O_{\mathcal{R}^2\mathcal{L}}$ still exists. As a consequence, in this region a variation of the parameter μ may cause dangerous border-collision bifurcations to occur. This is related with the existence of divergent orbits started at typical initial conditions, that means the existence of an attractor on the P.E..[7]

The second pair of regions, namely $\mathcal{P}_{\mathcal{RL}^2}^2$ and $\mathcal{P}_{\mathcal{R}^2\mathcal{L}}^2$, which does not exist for $\delta_{\mathcal{L}/\mathcal{R}} = 0$, shows a similar structure. Both regions are bounded by the non-smooth fold bifurcation curve $\xi_{\mathcal{RL}^2}^{\mathcal{L},1} \equiv \xi_{\mathcal{R}^2\mathcal{L}}^{\mathcal{R},1}$ defined by

$$\begin{aligned} \xi_{\mathcal{RL}^2}^{\mathcal{L},1} &= \left\{(\tau_{\mathcal{L}}, \tau_{\mathcal{R}}) \mid N_1^{\mathcal{RL}^2} = 0\right\} \\ &\equiv \left\{(\tau_{\mathcal{L}}, \tau_{\mathcal{R}}) \mid N_1^{\mathcal{R}^2\mathcal{L}} = 0\right\} = \xi_{\mathcal{R}^2\mathcal{L}}^{\mathcal{R},1}. \end{aligned} \tag{38}$$

As in the previous case, both orbits undergo P.E.-collision bifurcations at the curves $\chi_{\mathcal{RL}^2}$ and $\chi_{\mathcal{R}^2\mathcal{L}}$, respectively, and in the region between these curves dangerous border-collision bifurcations may occur.

Similar results can be obtained for further orbits from the $O_{\mathcal{RL}^n}$ family, whereby a pure analytical calculation is possible up to quite large values of n. As an example, Fig. 10 shows the regions of existence of the orbit $O_{\mathcal{RL}^3}$ and its complementary orbit $O_{\mathcal{R}^2\mathcal{L}^2}$. As one can see, both orbits emerge at the non-smooth fold bifurcation curve $\xi_{\mathcal{RL}^3}^{3,\mathcal{L}} \equiv \xi_{\mathcal{R}^2\mathcal{L}^2}^{0,\mathcal{R}}$. Hereby, the orbit $O_{\mathcal{RL}^3}$ may be stable or unstable (regions $\mathcal{P}_{\mathcal{RL}^3}^{1,s}$ and $\mathcal{P}_{\mathcal{RL}^3}^{1,u}$, respectively), whereas the orbit $O_{\mathcal{R}^2\mathcal{L}^2}$ is unstable in the complete region $\mathcal{P}_{\mathcal{R}^2\mathcal{L}^2}^1$. As the orbits $O_{\mathcal{RL}^2}$ and $O_{\mathcal{R}^2\mathcal{L}}$, also the orbits $O_{\mathcal{RL}^3}$ and $O_{\mathcal{R}^2\mathcal{L}^2}$ undergo P.E.-collision bifurcations (see the curves $\chi_{\mathcal{RL}^3}$ and $\chi_{\mathcal{R}^2\mathcal{L}^2}$ marked in Fig. 10). Again, the bifurcations curves $\xi_{\mathcal{RL}^3}^{3,\mathcal{L}} \equiv \xi_{\mathcal{R}^2\mathcal{L}^2}^{0,\mathcal{R}}$, $\chi_{\mathcal{RL}^3}$ and $\chi_{\mathcal{R}^2\mathcal{L}^2}$ intersect at the same codimension-2 bifurcation point. As a consequence, we observe a region in the parameter space where the stable orbit $O_{\mathcal{RL}^3}$ is already destroyed by a P.E.-collision bifurcation, whereas the unstable orbit $O_{\mathcal{R}^2\mathcal{L}^2}$ is not. Under variation of μ, this region may give rise to dangerous border-collision bifurcations associated with the periodic attractor $O_{\mathcal{RL}^2}^s$ and with a chaotic attractor.

The only difference between the situations with the orbits $O_{\mathcal{RL}^2}$, $O_{\mathcal{R}^2\mathcal{L}}$ and the orbits $O_{\mathcal{RL}^3}$, $O_{\mathcal{R}^2\mathcal{L}^2}$ is that the orbit $O_{\mathcal{RL}^3}$ has

[7] This subject depends also on the definition that one adopts for dangerous bifurcations because this definition may be associated with different dynamic behavior. For details, we refer to [43].

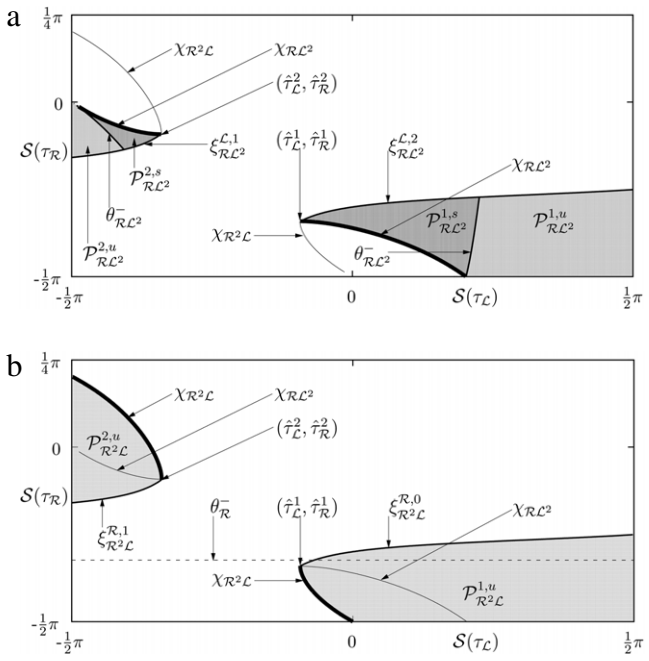

Fig. 9. Regions of existence of the period-3 orbits $O_{\mathcal{RL}^2}$ (a) and $O_{\mathcal{R}^2\mathcal{L}}$ (b) in the $(\tau_\mathcal{L}, \tau_\mathcal{R})$ parameter sub-space for $\delta_\mathcal{L} = \delta_\mathcal{R} = 0.55$. To indicate the region between the P.E.-collision curves where dangerous border-collision bifurcation may occur, the curves $\chi_{\mathcal{RL}^2}$ and $\chi_{\mathcal{R}^2\mathcal{L}}$ are repeated in both figures.

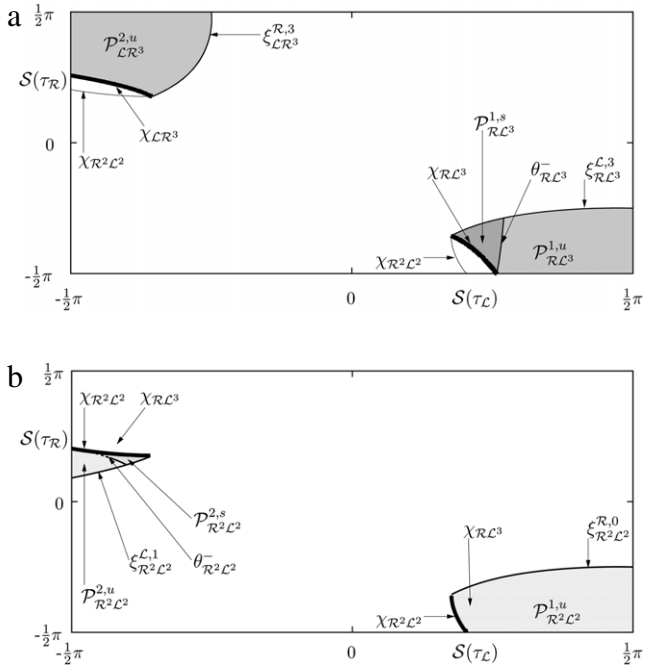

Fig. 10. Regions of existence of the period-4 orbits $O_{\mathcal{RL}^3}$ and $O_{\mathcal{R}^2\mathcal{L}^2}$ in the $(\tau_\mathcal{L}, \tau_\mathcal{R})$ parameter sub-space for $\delta_\mathcal{L} = \delta_\mathcal{R} = 0.55$. To indicate the region between the P.E.-collision curves where dangerous border-collision bifurcation may occur, the curves $\chi_{\mathcal{R}^2\mathcal{L}^2}$, $\chi_{\mathcal{RL}^3}$ and $\chi_{\mathcal{LR}^3}$ are repeated in both figures.

only one region of existence $\mathcal{P}^1_{\mathcal{RL}^3}$, whereas the orbit $O_{\mathcal{RL}^2}$ exists in two regions $\mathcal{P}^1_{\mathcal{RL}^2}$ and $\mathcal{P}^2_{\mathcal{RL}^2}$. This difference can be explained taking into account that the orbit $O_{\mathcal{RL}^2}$ represents a member of two families, namely $O_{\mathcal{RL}^n}$ (for $n = 2$) and $O_{\mathcal{R}^n\mathcal{L}^2}$ (for $n = 1$). In fact, the region $\mathcal{P}^1_{\mathcal{RL}^2}$ has the shape typical for the $O_{\mathcal{RL}^n}$ family, whereas the shape of the region $\mathcal{P}^2_{\mathcal{RL}^2}$ is typical for the $O_{\mathcal{R}^n\mathcal{L}^2}$ family.

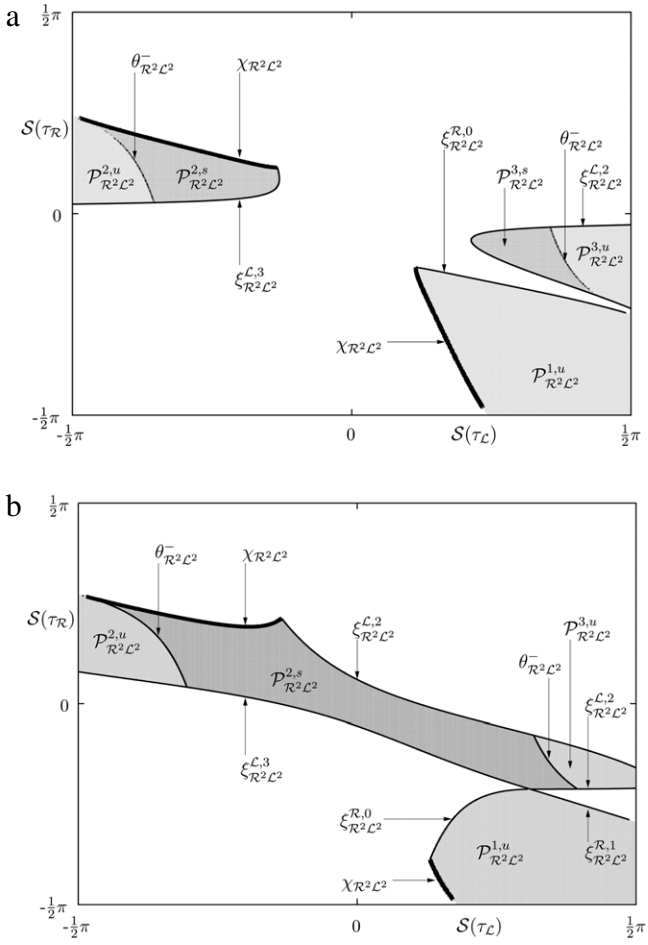

Fig. 11. Existence regions of the orbit $O_{\mathcal{R}^2\mathcal{L}^2}$ in the $(\tau_\mathcal{L}, \tau_\mathcal{R})$ parameter sub-space for $\delta_\mathcal{L} = \delta_\mathcal{R} = 0.92$ (a) and $\delta_\mathcal{L} = 0.4$, $\delta_\mathcal{R} = 1.32$ (b).

However, a detailed discussion of the $O_{\mathcal{R}^n\mathcal{L}^2}$ family is beyond the scope of this paper. Already known is that for increasing values of $\delta_{\mathcal{L}/\mathcal{R}}$ and n the number of regions of existence of these orbits increases. The curves bounding these regions are border-collision and P.E.-collision bifurcations. As an example, Fig. 11(a) shows three disjoint regions of the orbit $O_{\mathcal{R}^2\mathcal{L}^2}$. Under variation of $\delta_{\mathcal{L}/\mathcal{R}}$ these disjoint regions may also come to merging as shown in Fig. 11(b).

4.4. Codimension-2 bifurcation points

The results presented so far show that the boundaries of the existence regions of periodic orbits are given by two types of bifurcation curves, namely the border-collision bifurcation curves, where a point of the orbit collides with the boundary $x = 0$ and the P.E.-collision bifurcation curves, where the points tend to infinity. Therefore, the question that arises is how the investigated system behaves at the codimension-2 points where these two curves intersect. Considering the equations for specific orbits, we state that at the border-collision bifurcation curves the numerator of some periodic point becomes zero, whereas at the P.E.-collision bifurcation curves the denominators of all points becomes zero. Hence, at the codimension-2 bifurcation points we have an indeterminacy of type 0/0, and the question is what is the meaning of this indeterminacy for the system dynamics? It is worth noticing that the behavior at the codimension-2 bifurcation point depends on the type of the involved border-collision bifurcation which is a

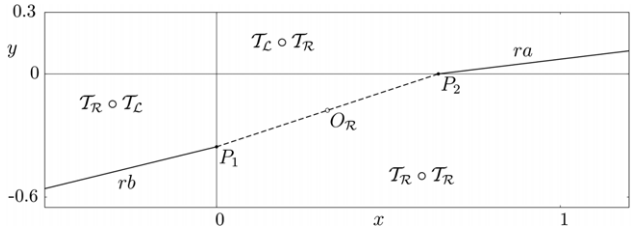

Fig. 12. Structure of the state space at the codimension-2 bifurcation point $(\hat\tau_\mathcal{L}, \hat\tau_\mathcal{R})$. The continuum of coexisting period-2 orbits located on the eigenvector of the fixed point O_R associated with the eigenvalue $\lambda_2^\mathcal{R} = -1$ is shown as a dashed line. The continuum of coexisting period-2 orbits $O_{\mathcal{RL}}$ located on the eigenvectors corresponding to the fixed points of the linear maps $\mathcal{T}_\mathcal{L} \circ \mathcal{T}_\mathcal{R}$ and $\mathcal{T}_\mathcal{R} \circ \mathcal{T}_\mathcal{L}$ associated with the eigenvalue $\lambda = +1$ is shown as solid line. It is also shown how the second iterated map is defined in several partitions of the state space. The boundaries between these partitions are given as thin lines $x = 0$ and $y = 0$. Parameter values are $\delta_\mathcal{L} = 0.15$, $\delta_\mathcal{R} = 0.55$.

degenerate flip bifurcation in the case of the two-cycle or a non-smooth fold bifurcation for all k-cycles with $k \geq 3$.

Let us consider first the intersection point of the degenerate flip bifurcation curve $\xi_{\mathcal{RL}}^{1,\mathcal{L}} \equiv \theta_\mathcal{R}^-$ and the P.E.-collision bifurcation curve $\chi_{\mathcal{RL}}$. From Eq. (22a) follows that this point is given by $(\hat\tau_\mathcal{L}, \hat\tau_\mathcal{R}) = (-\delta_\mathcal{L} - 1, -\delta_\mathcal{R} - 1)$ (see Fig. 6). Due to the degenerate flip bifurcation we have that the map $\mathcal{T}_\mathcal{R}$, and thus the fixed point $O_\mathcal{R}$ has an eigenvalue $\lambda_2^\mathcal{R} = -1$. As stated in Section 4.2, this leads to a segment of two-cycles, located on the eigenvector associated with that eigenvalue $\lambda_2^\mathcal{R} = -1$. This segment is bounded by the point P_1 where it contacts with the border of the phase plane $x = 0$ and by the point $P_2 = \mathcal{T}_\mathcal{R}(P_1)$ located at the line $y = 0$, as shown in Fig. 12. As all other points of this segment, the points P_1 and P_2 represent a two-cycle.

Recall that at the codimension-2 point $(\hat\tau_\mathcal{L}, \hat\tau_\mathcal{R})$ we have also the curve $\chi_{\mathcal{RL}}$, where the two-cycle $O_{\mathcal{RL}}$ undergoes a transcritical bifurcation on the P.E., associated with the eigenvalue $\lambda_1^{\mathcal{RL}} = +1$, as described in Section 4.2. Therefore, at this particular point the linear maps $\mathcal{T}_\mathcal{L} \circ \mathcal{T}_\mathcal{R}$ and $\mathcal{T}_\mathcal{R} \circ \mathcal{T}_\mathcal{L}$ associated with the points of the two-cycle $O_{\mathcal{RL}}$ have an eigenvalue $\lambda = +1$, with fixed points on the P.E. at the limit points of the corresponding eigenvectors of these linear maps. Consequently, the linear map $\mathcal{T}_\mathcal{R} \circ \mathcal{T}_\mathcal{L}$ (respectively, $\mathcal{T}_\mathcal{L} \circ \mathcal{T}_\mathcal{R}$) has one fixed point in P_1 (respectively, P_2) and one on the P.E., and due to $\lambda = +1$ this is possible only if each point on the whole segment is a fixed point. Thus, we have that the points on the eigenvectors associated with the eigenvalue $\lambda = +1$ of the two linear maps $\mathcal{T}_\mathcal{R} \circ \mathcal{T}_\mathcal{L}$ and $\mathcal{T}_\mathcal{L} \circ \mathcal{T}_\mathcal{R}$ are fixed points for these maps, all corresponding to the two-cycles of the map $\mathcal{T}$. Summarizing, the three straight lines in Fig. 12 are given by the eigenvectors associated with the eigenvalue $\lambda = +1$ of the three linear maps $\mathcal{T}_\mathcal{R} \circ \mathcal{T}_\mathcal{R}$, $\mathcal{T}_\mathcal{L} \circ \mathcal{T}_\mathcal{R}$ (the segment ra) and $\mathcal{T}_\mathcal{R} \circ \mathcal{T}_\mathcal{L}$ (the segment rb) and are loci of two-cycles of the map $\mathcal{T}$ at this codimension-2 point. It can be easily verified that $\mathcal{T}_\mathcal{R}(ra) = rb$ and $\mathcal{T}_\mathcal{L}(rb) = ra$.

Regarding the other codimension-2 points related with the k-cycles for $k \geq 3$ the bifurcation is completely different. The codimension-2 point represents in this case the intersection point of a non-smooth fold bifurcation curve and two P.E.-collision bifurcation curves. Let us describe in some detail the case $k = 3$ and the point $(\hat\tau_\mathcal{L}^1, \hat\tau_\mathcal{R}^1) = (-\delta_\mathcal{L}\delta_\mathcal{R}, -1/\delta_\mathcal{L})$ shown in Fig. 9.

At the non-smooth fold bifurcation curve $\xi_{\mathcal{RL}^2}^{\mathcal{L},2} \equiv \xi_{\mathcal{R}^2\mathcal{L}}^{\mathcal{R},0}$ at which a pair of 3-cycles appear, one periodic point is located on the line $x = 0$, then its image belongs to the line $y = 0$ and the third point to a line with the slope $m = -\delta_\mathcal{R}/\tau_\mathcal{R}$. Inserting Eq. (32) into Eqs. (29a) and (34a), we obtain the explicit coordinates of this 3-cycles:

$$x_i = \frac{N_i}{D}, \qquad y_i = \frac{M_i}{D}, \quad i = 0, 1, 2 \tag{39a}$$

with

$$N_0 = \mu(1 - \delta_\mathcal{L}), \qquad N_1 = \mu(1 + \tau_\mathcal{R}),$$
$$N_2 = 0, \qquad D = 1 + \delta_\mathcal{L}\tau_\mathcal{R}, \tag{39b}$$

$$M_0 = 0, \qquad M_1 = -\delta_\mathcal{R}N_0, \qquad M_2 = -\delta_\mathcal{L}N_1. \tag{39c}$$

It is worth noticing that for all parameter values on the non-smooth fold bifurcation curve, except the codimension-2 point, the values given by Eq. (39a) are finite. However, moving the parameters along the non-smooth fold bifurcation curve towards the codimension-2 point we observe that the point located on the boundary $x = 0$ (and hence its images) is moving towards the P.E. and at the codimension-2 point the 3-cycle belongs to the P.E. (the denominator D is vanishing in Eq. (39a)). Furthermore, at this codimension-2 point, besides the non-smooth fold bifurcation we have the intersection of the two other bifurcation curves (see Fig. 9) which represent the transcritical P.E.-collision bifurcations of both 3-cycles, as shown in Section 4.3. Consequently, at the codimension-2 bifurcation the single 3-cycle located at the P.E. has one eigenvalue $+1$. The same behavior occurs at the other codimension-2 point $(\hat\tau_\mathcal{L}^2, \hat\tau_\mathcal{R}^2) = (-1/\delta_\mathcal{R}, -\delta_\mathcal{L}\delta_\mathcal{R})$ of the 3-cycles, and at the codimension-2 points caused by non-smooth fold and transcritical P.E.-collision bifurcations of other k-cycles with $k > 3$.

5. Summary and outlook

When dealing with piecewise-smooth systems, it will be typically stated that periodic orbits of these systems may undergo two types of bifurcations. The first type of bifurcations occur in smooth systems as well (for example saddle–node, flip, and so on) and are, therefore, not specific for piecewise-smooth systems. By contrast, the second type represents bifurcations which occur at the boundary between several partitions in the state space (border- and corner-collisions, sliding, and so on) and are, therefore, specific for piecewise-smooth systems. Although this is correct, it will be often overseen how the partitions in the state space are defined. For example, in the case that a system is defined in two partitions $x < 0$ and $x > 0$, then a more correct way to specify the partitions is to say that they are given by the open intervals $(-\infty, 0)$ and $(0, +\infty)$. Thus, it becomes clear that not only the point $x = 0$ but also the point $\pm\infty$ represents a boundary between the partitions. As in the case of a collision with a finite boundary, an orbit undergoing a collision with the boundary at infinity becomes virtual. These bifurcations, denoted as P.E. collision bifurcations, show all properties typical for border-collision bifurcations except that the involved boundary in the state space is located at infinity. The main advantage of this concept is that it leads to a unified representation of bifurcations occurring at both, the finite boundaries in the state space and at infinity.

Furthermore, we extended a result already mentioned in [28] and demonstrated that in the case of piecewise-linear maps the P.E.-collision bifurcations occur at the stability boundary, where one of the eigenvalues of the corresponding Jacobian matrix becomes $+1$. Originally stated for the basic orbits of the 2D continuous normal form, this result is proven for any orbits of any piecewise-linear maps, independent of the state space dimension, number of partitions and whether the map is continuous or not.

As an application example, we demonstrated the relevance of the P.E.-collision bifurcations for understanding the bifurcation structures in the continuous 1D and 2D piecewise-linear normal form. In the case of the 1D normal form, only the fixed points and the period-2 orbit undergo P.E.-collision bifurcations, whereas the regions of existence of other periodic orbits are bounded by usual border-collision bifurcation curves. In contrast to this, in the case of the 2D normal form the regions of existence of other periodic orbits are bounded by bifurcation curves of both types, that means

border- as well as P.E.-collision bifurcations. It was already known that the border-collision bifurcations for k-cycles with $k \geq 3$ are of the non-smooth fold type. The case $k = 2$ is a special case where the border-collision bifurcation represents a degenerate flip bifurcation. We demonstrated additionally that the points on the P.E. where the eigenvectors of a finite fixed point are tending to, represent fixed points also, and that the same argument can be applied for orbits with any periods. At the P.E.-collision bifurcation a finite orbit and an orbit on the P.E. merge and interchange their stability, so we conclude that this bifurcation represents a transcritical bifurcation occurring on the P.E.. This bifurcation has an additional feature, namely that one of the involved orbits becomes virtual after the bifurcation.

Since the existence region of a periodic orbit is typically bounded by more than one bifurcation curve, at the intersection points of these curves we observe codimension-2 bifurcations. They may be caused by the intersection of two usual border-collision bifurcation curves and represent in this case a usual codimension-2 border-collision bifurcation, where two points of the involved orbit collide with the boundary $x = 0$ simultaneously, or by the intersection of a border-collision and a P.E.-collision bifurcation curve. In the last case, we have demonstrated that for k-cycles with $k \geq 3$ this codimension-2 bifurcation represent a non-smooth fold bifurcation occurring at the P.E.. In the case of the two-cycle, the situation is different and at the codimension-2 bifurcation point we observe a continuum of orbits.

Appendix. Fixed points on the P.E.

Let us consider the linear map $X_{n+1} = L(X_n) = AX_n$, where $A = \begin{pmatrix} \tau & 1 \\ -\delta & 0 \end{pmatrix}$, i.e.

$$\begin{aligned} x_{n+1} &= \tau x_n + y_n \\ y_{n+1} &= -\delta x_n \end{aligned} \tag{40}$$

(then we can apply the results to $\mathcal{T}_{\mathcal{L}}$ and/or $\mathcal{T}_{\mathcal{R}}$). The points on the P.E. of the linear map L are obtained considering the change of variables (see [20,21])

$$x = \frac{1}{z}, \qquad y = \frac{s}{z}. \tag{41}$$

Thus, we get the map:

$$\begin{aligned} z_{n+1} &= \frac{z_n}{\tau + s_n} \\ s_{n+1} &= -\frac{\delta}{\tau + s_n} \end{aligned} \tag{42}$$

whose fixed points are obtained by solving the equations $z_{n+1} = z_n$ and $s_{n+1} = s_n$, and those on the P.E. are obtained for $z = 0$. As it is $s = \frac{y}{x}$ we have for map (40) that the values of s give the slopes of the eigenvectors of the fixed point at the origin which tend to the points on the P.E.. For $z = 0$, we get

$$s = s_{\pm} = -\frac{\tau \pm \sqrt{\tau^2 - 4\delta}}{2} \tag{43}$$

and the fixed points on the P.E. may be represented as points on the circle, or referring to the phase plane: they are the limit points of the lines having the slopes s.

With the transformation used above, we cannot analyze the points at infinity on the y-axis. In this case, we have to use the following transformation

$$x = \frac{\xi}{\eta}, \qquad y = \frac{1}{\eta} \tag{44}$$

obtaining the map:

$$\begin{aligned} \eta_{n+1} &= -\frac{\eta_n}{\xi_n \delta} \\ \xi_{n+1} &= -\frac{\xi_n \tau + 1}{\xi_n \delta} \end{aligned} \tag{45}$$

and the points on the P.E. are obtained for $\eta = 0$. The values of $\xi = \frac{x}{y}$ give now the inverse of the slopes of the eigenvectors of the fixed point at the origin which tend to the points on the P.E.. For $\eta = 0$, we obtain

$$\xi = \xi_{\pm} = -\frac{\tau \pm \sqrt{\tau^2 - 4\delta}}{2\delta} \tag{46}$$

so that the fixed points on the P.E. may be represented as points on the circle, corresponding to the lines with the slopes

$$s_{\pm} = \frac{1}{\xi_{\pm}} = -\frac{2\delta}{\tau \pm \sqrt{\tau^2 - 4\delta}}. \tag{47}$$

All this comes from the theory. Now, we prove the following

Proposition. *The fixed points on the P.E. of a linear or affine map with real eigenvalues are the limit points of the eigenvectors of the fixed point at the origin.*

Proof. Consider the linear map $X_{n+1} = L(X_n) = AX_n$ for which the fixed point is in the origin and its stability is studied via the eigenvalues, solution of the equation

$$\lambda^2 - \tau\lambda + \delta = 0 \tag{48}$$

that is:

$$\lambda_{\pm} = \frac{\tau \pm \sqrt{\tau^2 - 4\delta}}{2} \tag{49}$$

then the related eigenvectors are given by

$$r_{\pm} = \begin{pmatrix} 1 \\ \lambda_{\pm} - \tau \end{pmatrix} = \begin{pmatrix} 1 \\ -\frac{\delta}{\lambda_{\pm}} \end{pmatrix}. \tag{50}$$

As the eigenvectors are fixed lines, to prove the proposition it is enough to prove that the slopes of the eigenvectors are the same as obtained above. From (50), we have $m_{\pm} = \frac{y}{x} = \lambda_{\pm} - \tau = -\frac{\delta}{\lambda_{\pm}}$ and from the expression of the eigenvalues in (49) we obtain

$$m_{\pm} = \lambda_{\pm} - \tau = -\frac{\tau \pm \sqrt{\tau^2 - 4\delta}}{2} = s_{\pm} \tag{51}$$

and also

$$m_{\pm} = \frac{y}{x} = -\frac{\delta}{\lambda_{\pm}} = -\frac{2\delta}{\tau \pm \sqrt{\tau^2 - 4\delta}} = s_{\pm}. \tag{52}$$

In the affine case, when the map has a constant term, then the position of the fixed point in the phase plane is no longer in the origin, but this does not change the analysis performed above, as via a translation we obtain the previous case and we have the same formulas as above. Thus, considering the eigenvectors issuing from the related fixed point, their limit points give the fixed points on the P.E., which completes the proof. □

References

[1] R. Burridge, L. Knopoff, Model and theoretical seismicity, Bull. Seismol. Soc. Amer. 57 (3) (1967) 341–371.
[2] J. Nussbaum, A. Ruina, A two degree-of-freedom earthquake model with static/dynamic friction, J. Pure Appl. Geophys. 125 (4) (1987) 629–656. doi:10.1007/BF00879576.
[3] M. Mita, M. Arai, S. Tensaka, D. Kobayashi, H. Fujita, A micromachined impact microactuator driven by electrostatic force, J. Microelectromech. Syst. 12 (2003) 37–41. doi:10.1109/JMEMS.2002.802906.
[4] X. Zhao, H. Dankowicz, C.K. Reddy, A.H. Nayfeh, Modeling and simulation methodology for impact microactuators, J. Micromech. Microeng. 14 (2004) 775–784. doi:10.1088/0960-1317/14/6/003.

[5] H. Dankowicz, X. Zhao, Local analysis of co-dimension-one and co-dimension-two grazing bifurcations in impact microactuators, Physica D 202 (2005) 238–257. doi:10.1016/j.physd.2005.02.008.
[6] X. Zhao, H. Dankowicz, Unfolding degenerate grazing dynamics in impact actuators, Nonlinearity 19 (2006) 399–418. doi:10.1088/0951-7715/19/2/009.
[7] S. Banerjee, G.C. Verghese, Nonlinear Phenomena in Power Electronics — Attractors, Bifurcations, Chaos, and Nonlinear Control, IEEE Press, 2001.
[8] Zh. T. Zhusubaliyev, E. Mosekilde, Bifurcations and Chaos in piecewise-smooth dynamical systems, in: Nonlinear Science A, vol. 44, World Scientific, 2003.
[9] A.B. Nordmark, Non-periodic motion caused by grazing incidence in an impact oscillator, J. Sound Vibration 145 (2) (1991) 279–297.
[10] H. Dankowicz, A.B. Nordmark, On the origin and bifurcations of stick–slip oscillations, Physica D 136 (2000) 280–302.
[11] E. Sontag, Mathematical Control Theory: Deterministic Finite Dimensional Systems, 2nd ed., in: Texts in Applied Mathematics, vol. 6, Springer Verlag, NY, 1998.
[12] T. Puu, L. Gardini, I. Sushko, Cournot duopoly with kinked demand according to Palander and Wald, in: T. Puu, I. Sushko (Eds.), Oligopoly Dynamics, Models and Tools, Springer Verlag, 2002, pp. 111–146 (Chapter 5).
[13] A. Agliari, G.I. Bischi, L. Gardini, Some methods for the global analysis of closed invariant curves in two-dimensional maps, in: T. Puu, I. Sushko (Eds.), Business Cycle Dynamics — Models and Tools, Springer Verlag, 2006, pp. 7–47 (Chapter 1).
[14] P. Tracqui, Organizing centres and symbolic dynamic in the study of mixed-mode oscillations generated by models of biological autocatalytic processes, Acta Biotheoret. 42 (1994) 147–166.
[15] D. Lyubimov, A. Pikovsky, M. Zaks, Universal Scenarios of Transitions to Chaos via Homoclinic Bifurcations, in: Math. Phys. Rev., vol. 8, Harwood Academic, London, 1989.
[16] E.N. Lorenz, Deterministic non-periodic flows, J. Atmospheric Sci. 20 (1963) 130.
[17] H.E. Nusse, J.A. Yorke, Border-collision bifurcations including 'period two to period three' bifurcation for piecewise smooth systems, Physica D 57 (1992) 39–57.
[18] H. Poincaré, Mémoire sur les courbes définiés par une équation differentielle, J. de Math. 7 (1981) 375–422.
[19] M. di Bernardo, C.J. Budd, A.R. Champneys, P. Kowalczyk, Piecewise-Smooth Dynamical Systems: Theory and Applications, in: Applied Mathematical Sciences, vol. 163, Springer, 2007.
[20] S. Lefschetz, Differential Equations: Geometric Theory, Interscience, 1957.
[21] A.A. Andronov, E.A. Leontovich, I.I. Gordon, A.G. Majer, Qualitative Theory of Second-Order Dynamical Systems, John Wiley & Sons, NY, 1973.
[22] E.A. Gonzalez-Velasco, Generic properties of polynomial vector fields at infinity, Trans. Amer. Math. Soc. 143 (1969) 201–222.
[23] J. Llibre, D.G. Saari, Periodic orbits for the planar newtonian three-body problem coming from the elliptic restricted three-body problems, Trans. Amer. Math. Soc. 347 (1995) 3017–3030.
[24] T. Iwai, The Poincaré compactification of the mickepler problem with positive energies, J. Phys. A: Math. Gen. 34 (2001) 1713–1723.
[25] E. Kappos, Dynamics of polynomial systems at infinity, Electron. J. Differential Equations 2001 (22) (2001) 1–15.
[26] A. Garcia, E. Pérez-Chavela, A. Susin, A generalization of the Poincaré compactification, Arch. Ration. Mech. Anal. 179 (2006) 285–302.
[27] H. Bai-Lin, Elementary Symbolic Dynamics and Chaos in Dissipative Systems, World Scientific Publishing, 1989.
[28] A. Ganguli, S. Banerjee, Dangerous bifurcation at border collision: when does it occur? Phys. Rev. E 71 (2005) 057202.
[29] Y.L. Maistrenko, V.L. Maistrenko, L.O. Chua, Cycles of chaotic intervals in a time—delayed Chua's circuit, Internat. J. Bifur. Chaos 3 (6) (1993) 1557–1572.
[30] Y.L. Maistrenko, V.L. Maistrenko, S.I. Vikul, L.O. Chua, Bifurcations of attracting cycles from time-delayed Chua's circuit, Internat. J. Bifur. Chaos 5 (3) (1995) 653–671.
[31] H.E. Nusse, J.A. Yorke, Border-collision bifurcations for piecewise smooth one dimensional maps, Internat. J. Bifur. Chaos 5 (1) (1995) 189–207.
[32] M. Dutta, H.E. Nusse, E. Ott, J.A. Yorke, G. Yuan, Multiple attractor bifurcations: a source of unpredictability in piecewise smooth systems, Phys. Rev. Lett. 83 (1999) 4281–4284.
[33] M. di Bernardo, M.I. Feigin, S.J. Hogan, M.E. Homer, Local analysis of C-bifurcations in n-dimensional piecewise smooth dynamical systems, Chaos Solitons Fractals 10 (1999) 1881–1908.
[34] Zh.T. Zhusubaliyev, E. Mosekilde, Equilibriun-torus bifurcation in nonsmooth system, Physica D 237 (2008) 930–936.
[35] Zh.T. Zhusubaliyev, E. Mosekilde, S. Banerjee, Multiple-attractor bifurcations and quasiperiodicity in piecewise-smooth maps, Internat. J. Bifur. Chaos 18 (6) (2008) 1775–1789.
[36] M.I. Feigin, On the structure of C-bifurcation boundaries of piecewise-continuous systems, Prikl. Math. Mekh. 42 (1978) 820–829 (in Russian).
[37] M.I. Feigin, Forced Oscillations in Systems with Discontinuous Nonlinearities, Nauka Publ., Moscow, 1994 (in Russian).
[38] S. Banerjee, C. Grebogi, Border collision bifurcation in two-dimensional piecewise smooth maps, Phys. Rev. E 59 (1999) 4052–4061.
[39] J. Guckenheimer, P.J. Holmes, Nonlinear Oscillations, Dynamical Systems and Bifurcations of Vector Fields, 4th ed., in: Applied Mathematical Sciences, Springer, 1993.
[40] I. Sushko, L. Gardini, Degenerate bifurcations and border collisions in piecewise smooth 1D and 2D maps, Internat. J. Bifur. Chaos (2010) (in press).
[41] M.A. Hassouneh, E.H. Abed, H.E. Nusse, Robust dangerous border-collision, Phys. Rev. Lett. 92 (2004) 070201.
[42] I. Sushko, L. Gardini, Center bifurcation for a two-dimensional border-collision normal form, Internat. J. Bifur. Chaos 18 (4) (2008) 1029–1050.
[43] L. Gardini, V. Avrutin, M. Schanz, Connection between bifurcations on the Poincaré equator and dangerous bifurcations, in: A. Sharkovsky, I. Sushko (Eds.), Iteration Theory, in: Grazer Math. Ber., 2009, pp. 53–72.
[44] W. Chin, E. Ott, H.E. Nusse, C. Grebogi, Grazing bifurcations in impact oscillators, Phys. Rev. E 50 (6) (1994) 4427–4444.
[45] F. Casas, W. Chin, C. Grebogi, E. Ott, Universal grazing bifurcations in impact oscillators, Phys. Rev. E 53 (1996) 134–139.
[46] V. Avrutin, M. Schanz, S. Banerjee, Multi-parametric bifurcations in a piecewise-linear discontinuous map, Nonlinearity 19 (2006) 1875–1906.